Climate Extremes and Variability Surrounding Chesapeake Bay: Past, Present, and Future

Kari A. St.Laurent (iD) *, Victoria J. Coles* (iD) *, and Raleigh R. Hood* (iD)

Research Impact Statement: Temperature and precipitation extremes have changed over the past century near the Chesapeake Bay, and models project continued climate change modulated by natural variability.

ABSTRACT: Measures of extreme climate variability around Chesapeake Bay have changed over the past century (1895–2014), resulting in the need to establish new baselines for understanding future change. Here, observed climate variability is compared with Coupled Model Intercomparison Project fifth assessment climate models to evaluate ensemble model skill in this region. Observed trends include annual and seasonal declines in the percentage of cold days. Similarly, increases in the annual and seasonal percentages of warm days occurred in all seasons of the North Chesapeake (>38.2°N) but were only significant in spring and summer in the South (<38.2°N) demonstrating regional differences even at local scales. Precipitation intensity increased over the past century. Models using emissions scenarios RCP4.5 and 8.5 project these trends will continue, though they have little skill in precipitation extremes. Pacific and Atlantic climate modes are generally more correlated with climate extremes than mean temperature and precipitation suggesting potential predictability in the synoptic patterns underlying the extremes. However, they also drive the need for time series at least 60-years long for establishing climate trends. This local analysis differs from regional, state level, and local 2.5° × 3.75° grid analyses, highlighting the importance of local climate assessments that consider topographic and regional weather patterns.

(KEYWORDS: climate variability; climate extreme change; National Estuarine Research Reserve System; Chesapeake Bay.)

INTRODUCTION

The continental United States (U.S.) annual mean surface air temperature has increased by 0.72°C to 1.06°C since 1895 and annual precipitation has increased by 5% since 1900 (Melillo et al. 2014). However, these trends in average temperature and precipitation may not reflect the day to day environmental variability experienced by ecosystems. Climate extremes (i.e., events with an annual to sub-annual re-occurrence time, Zhang et al. 2011) play a role in influencing human health, ecological tipping points, and environmental boundaries (Karl et al. 1999; Peterson et al. 2001). As a result, 26 measures for climate events were developed by the Expert Team for Climate Change Detection and Indices (ETCCDI) that can be applied to global and regional model output as well as to localized daily weather station data (Karl et al. 1999, 2009; Peterson et al. 2001). These extreme

climate indices express the intensity, duration, and frequency of temperature- and precipitation-based events.

Chesapeake Bay is the largest estuary in the U.S. and is particularly sensitive to changes in climate extremes since the Bay is shallow, with a mean depth <6.5 m (Kemp et al. 2005), leading to tight coupling between water-column and atmospheric variability (Austin 2002; Ding and Elmore 2015). In many climate assessments, such as the Intergovernmental Panel on Climate Change (IPCC) and U.S. Global Change Research Program, the Bay is subdivided into the Northeast and Southeast regions at the Maryland-Virginia border (Horton et al.) making it challenging to interpret climate projections for Chesapeake Bay-specific purposes. In regional analyses, precipitation quantity and intensity in the spring and winter seasons are projected to increase, followed by periods of extended drought, drastically affecting streamflow and stormwater runoff into Chesapeake Bay (Pyke et al. 2008; Najjar et al. 2010). These analyses, however, typically use spatially large regions such as the entire Chesapeake Bay watershed to characterize expected trends, which are appropriate for streamflow, but which may not be relevant to conditions in the estuary itself. Local assessment of climate change and variability in the Chesapeake Bay is needed for determining ecological vulnerability.

Climate extreme events are particularly relevant to the physiological thresholds of specific organisms, such as eelgrass (*Zostera marina*), which has experienced diebacks in the Chesapeake Bay when water temperatures exceeded 30°C for prolonged periods (Moore and Jarvis 2008). Similarly, seasonal extremes often define the environmental boundaries of organisms, possibly allowing for shifts in the range of nonindigenous species, such as recent observations of a northward expansion of the southern flounder, *Paralichthys lethostigma*, and the brown pelican, *Pelecanus occidentalis* (Najjar et al. 2010; Lusk et al. 2014). Changes in precipitation intensity or frequency can affect the probability of nuisance flooding and nutrient runoff into the Bay as well as lead to large salinity swings (Pyke et al. 2008; Najjar et al. 2010). Runoff from precipitation events may be amplified by increases in impervious surfaces that lead to increased volume of wastewater generated (Claggett et al. 2013). Thus, water quality in the Chesapeake Bay is influenced not just by mean thermal and precipitation patterns, but also by local heat spells, intense and flashy thunderstorms with high runoff, and by the temporal changes in growing season that may cause a mismatch between plant and animal growth timing.

Here, we present a historical, data-driven assessment of the past and present climate extremes as well as model-derived future projections of extreme temperature- and precipitation-related events specific to the Chesapeake Bay near-shore region. Our main goal is to assess how local climate, manifested in extreme events at the seasonal and annual scale, has changed over the past century, and to establish the present-day baselines against which future changes can be assessed. In addition, we use the historical record to assess model skills in predicting past extremes in order to develop confidence estimates for model predictions of future change near the Chesapeake Bay. Finally, we relate trends in the climate extremes and their covariance to large scale climate modes to assess their predictability and interaction for future model assessments and consider the implications for oxygen concentrations which form the basis for policy interventions such as the Total Maximum Daily Load (e.g., Irby et al. 2018).

METHODS

Data Description

Climate extremes were evaluated in the Chesapeake Bay near-shore region using 25 of the 26 IPCC extreme climate indices defined by the ETCCDI (Peterson et al. 2001; Alexander et al. 2006; Karl et al. 2009; Table 1). These indices were calculated using three datasets as inputs: a 2.5° × 3.75° gridded HadEX2 data product, daily weather stations from the National Oceanic and Atmospheric Administration's National Centers for Environmental Information's Global Historical Climate Network (GHCN-Daily), and future projections from the Phase 5 Coupled Model Intercomparison Project (CMIP5) multi-model ensemble (Table 2).

The climate extreme indices calculated from the HadEX2 data product were downloaded from the CLIMDEX program (http://www.climdex.org/index.html). The HadEX2 dataset is available from 1901 to 2010 and is based primarily on GHCN-Daily data within the grid cell of interest (Alexander et al. 2006; Donat et al. 2013a). A single gridpoint was extracted from the HadEX2 over the Chesapeake Bay near-shore region (longitude: −75 to −78.75°W, latitude 40 to 37.5°N). This grid cell is highlighted in Figure 1.

Three ensembles of GHCN-Daily weather stations were assessed in this study, a small hand-selected ensemble, the U.S. Historical Climatology Network stations, and a third group that includes all GHCN-Daily weather stations below 60 m, with at least a 10-year record, and located within Maryland and Virginia and within −77.5° to −75.5° longitude (146

TABLE 1. Temperature- and precipitation-based climate extreme index definitions, units, and classification (intensity, frequency, or duration).

Type	Extreme event index	Type	Units	Definition
Cold	Icing Days (ID)	Frequency	days	Annual count of days when $T_{max} < 0°C$
Cold	Frost Days (FD)	Frequency	days	Annual count of days when $T_{min} < 0°C$
Cold	TX10p*	Frequency	%days	Percentage of days when $T_{max} < 10$th percentile
Cold	TN10p*	Frequency	%days	Percentage of days when $T_{min} < 10$th percentile
Cold	TXn*	Intensity	°C	Lowest daily T_{max}
Cold	TNn*	Intensity	°C	Lowest daily T_{min}
Cold	Cold Spell Duration Index (CSDI)	Duration	days	Annual count of at least six consecutive days when $T_{min} < 10$th percentile
Warm	Summer Days (SU)	Frequency	days	Annual count of days when $T_{max} > 25°C$
Warm	Tropical Nights (TR)	Frequency	days	Annual count of days when $T_{min} > 20°C$
Warm	Growing Season Length (GSL)	Duration	days	Annual calendar count of days between the first six consecutive days with $T_{mean} > 5°C$ and first occurrence of consecutive six days when $T_{mean} < 5°C$
Warm	TX90p*	Frequency	%days	Percentage of days when $T_{max} > 90$th percentile
Warm	TN90p*	Frequency	%days	Percentage of days when $T_{min} > 90$th percentile
Warm	TXx*	Intensity	°C	Highest daily T_{max}
Warm	TNx*	Intensity	°C	Highest daily T_{min}
Warm	Warm Spell Duration Index (WSDI)	Duration	days	Annual count of at least six consecutive days when $T_{max} > 90$th percentile
Dry	Consecutive Dry Days (CDD)	Duration	days	Maximum annual count of consecutive dry days
Precip	R10mm	Frequency	days	Annual count of days with >10 mm precipitation
Precip	R20mm	Frequency	days	Annual count of days with >20 mm precipitation
Precip	Rx1day*	Intensity	mm	Maximum one-day precipitation amount
Precip	Rx5day*	Intensity	mm	Maximum five-day precipitation amount
Precip	Simple Daily Intensity Index (SDII)	Intensity	mm/day	Total annual precipitation/count of wet days (>1.0 mm)
Precip	R95p	Intensity	mm	Annual sum of daily precipitation which exceeds the 95th percentile
Precip	R99p	Intensity	mm	Annual sum of daily precipitation which exceeds the 99th percentile
Precip	Total Annual Precipitation (PRCPTOT)	Intensity	mm	Annual sum of precipitation (days with >1.0 mm)
Precip	Consecutive Wet Days (CWD)	Duration	days	Maximum annual count of CWD

Note: The asterisk denotes indices which are calculated seasonally.

TABLE 2. List of global climate model names, resolution the data are reported at, the grid cell used, and the institutions associated with each model group used to project the future climate extreme trends in the near-shore Chesapeake region.

Model	Resolution provided	Grid cell used	Associated institutions
ACCESS1.0	Atmosphere Lon: ~1.875° Lat: ~1.25°	Lon:152, Lat:104	Commonwealth Scientific and Industrial Research Organization (CSIRO) and Bureau of Meteorology CSIRO-BOM (BOM), Australia
CCSM4	Atmosphere Lon: ~1.25° Lat: ~0.9°	Lon:228, Lat: 137	National Center for Atmospheric Research
CMCC-CM	Atmosphere Lon: ~.075° Lat: ~0.75°	Lon:379, Lat:172	Centro Euro-Mediterraneo per I Cambiamenti Climatici
HadGEM2-ES	Atmosphere Lon: ~1.875° Lat: ~1.25°	Lon:152, Lat:104	Met Office Hadley Centre (HadGEM2-ES realizations contributed by Instituto Nacional de Pesquisas Espaciais)
MIROC5	Atmosphere Lon: ~1.4° Lat: ~1.4°	Lon:202, Lat:92	Atmosphere and Ocean Research Institute (The University of Tokyo), National Institute for Environmental Studies, and Japan Agency for Marine-Earth Science and Technology
MPI-ESM-MR MPI-ESM-LR	Atmosphere Lon: ~1.875° Lat: ~1.875° Atmosphere Lon: ~1.875° Lat: ~1.875°	Lon:152, Lat: 69	Max-Planck-Institut für Meteorologie (Max Planck Institute for Meteorology)
MRI-CGCM3	Atmosphere Lon: ~1.125° Lat: ~1.125°	Lon:252, Lat:114	Meteorological Research Institute

stations in total). The second and third groups were more similar in climate normals and trends than the first, so they were judged to be more reliable. Using the third larger ensemble provides more spatially inclusive results (Figure 1; Table S1) and is used for all further analyses. Each station was visually inspected for obvious anomalies, and these periods of the record were removed from the data for four stations.

The data from GHCN-Daily stations were retained only if the quality flag was not questionable, and gaps of up to seven days were filled using linear interpolation (package zoo, function na.approx Zeileis and Grothendieck 2005). The climate extreme indices were calculated for each station using the default values in the R climdex.pcic package (Bronaugh 2018). A minimum criterion of at least 75% of daily weather data present was established for calculating annual and seasonal indices for each year. The stations were grouped into North Chesapeake or South Chesapeake using latitude 38.2°N as the regional separator. The groups of time series were averaged using equal weighting for duration and frequency indices. For intensity indices, averaging strongly reduces the intensity of events, thus the 90th and 10th percentile of the ensemble at each time were used for warm and cold intensity indices, respectively. The monthly time series were further aggregated into seasons using the same procedure and only seasonal time series are presented.

Time series of extreme event indices (Peterson et al. 2001) from the IPCC CMIP5 multi-model ensemble were obtained from the Canadian Center for Climate Modeling and Analysis (http://www.ccc ma.ec.gc.ca/data/climdex/index.shtml). A global analysis comparing the individual model performance with model reanalysis products was used to select eight models whose global skill is better than average compared with reanalysis products and for which the extreme indices were available (Sillmann et al. 2013) (Figure 10). Two climate scenarios, RCP4.5 and RCP8.5, were evaluated (Moss et al. 2010). In RCP4.5, carbon dioxide emissions peak around 2040, then decline. In RCP8.5, emissions continue to increase throughout the 21st Century. While other representative concentration pathway scenarios present more drastic policy interventions and could perhaps inspire greater interest in reducing local emissions, we chose here to bracket more realistic future pathways rather than aspirational pathways in order to provide ecologically relevant potential futures for planning purposes. The 1981–2010 climate normal mean for each model was replaced with the 1981–2010 observational mean for the grouped North and South Chesapeake GHCN-Daily stations to remove annual, but not seasonal, individual model bias.

Present Day Baseline Establishment

Climate normals (30-year climatological mean from 1981 to 2010; Table 3) were used as the present-day baseline. This period is the current climate normal used by the NOAA National Centers for Environmental Information. These values were also used for determining the percentage change in climate extremes over the past decades and century.

Analysis and Confidence Assessment

The short-term change was assessed using shifts in the probability distribution function (PDFs). Changes in the PDFs for the climate indices were calculated using the kernel density function in R and assessed using a two-sided Anderson-Darling test (package kSamples, ad.test, Scholz and Zhu 2019) to determine whether the distribution functions for 1951–1980 and 1981–2010 (past) or 1981–2010 and 2010–2040 (future) were drawn from the same unknown underlying distribution. The PDFs between these two reference periods were considered to be statistically different when the p-value is <0.05.

The significance of the historical trend (~115 years) for the HadEX2 time series, the aggregated North and South Chesapeake region time series, and the past and future trends (1900–2006 and 2006–2100) in the climate model time series were assessed using: linear regression of the filtered time series (21-year centered moving mean); Sen's method of computing the median of the ensemble of point by point linear slopes (package trend, sens.slope, Pohlert 2018); and a Mann–Kendall test on the filtered time series (package Kendall, McLeod 2011). The statistical tests were considered significant if the p-value is <0.05. A level of confidence in the observed and modeled past and future trends was assigned depending on the significance of each test: Level 4 (strong confidence, all linear model and Mann–Kendall tests were significant in trend and linear model and Sen's slope have same directionality); Level 3 (high confidence, one test was significant with same sign slope in both methods); Level 2 (low confidence, two tests were significant with different directionality); Level 1 (low confidence, one trend was significant); Level 0 (low confidence, no trends are significant). To reduce complexity, we only provide one measure of low confidence for Levels 2, 1, and 0 in tables. Percentage changes are calculated in decadal trend divided by the climate normal to provide a sense of the magnitude of the changes relative to the climate normal.

Model-based consensus must be expressed differently because we include an ensemble of models in the analysis as opposed to the datasets where there
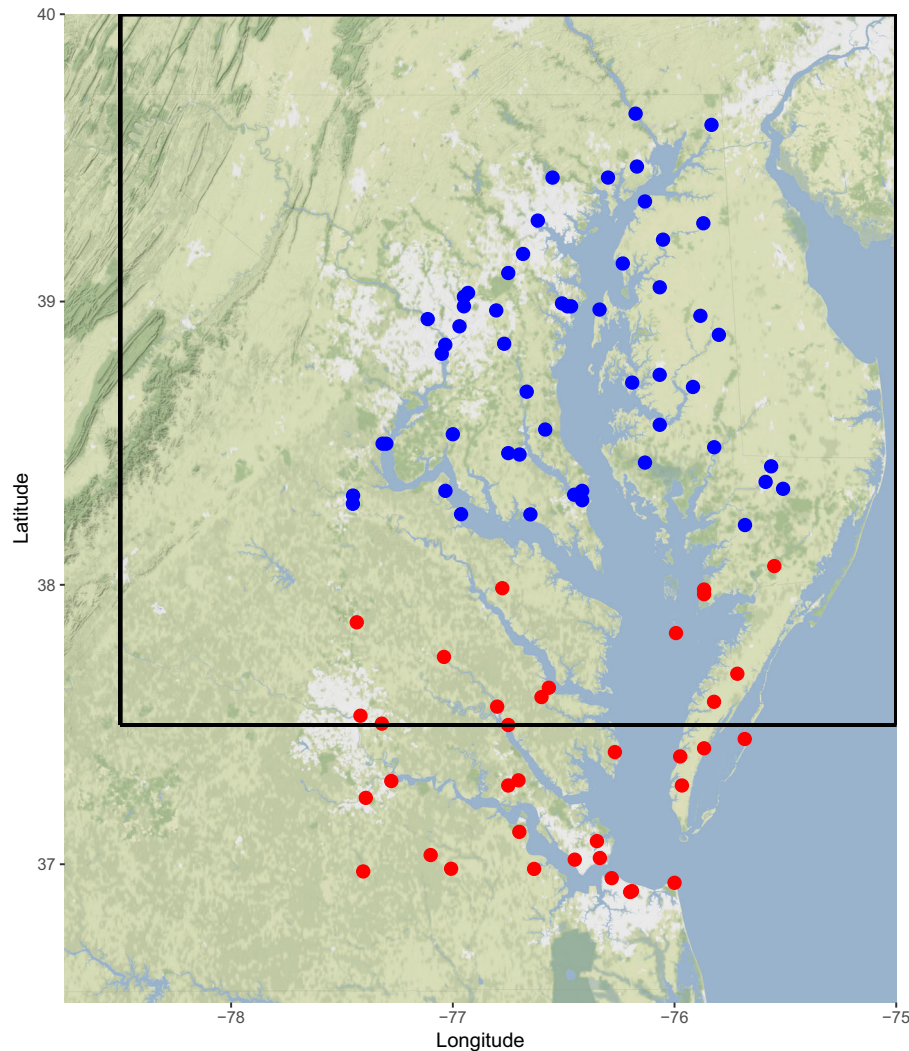
FIGURE 1. Map of the study region. Blue and red circles denote the North and South Chesapeake Global Historical Climate Network-Daily weather stations, respectively. The black square spans the grid size of the HadEX2 data product.

is a single analyzed time series. Consensus is expressed following the methods of Tebaldi et al. (2011): Case 1 (low consensus) occurs when <50% of model trends were statistically significant; Case 2 (greater consensus) occurs when >50% of model trends were statistically significant and <75% of the models agreed on the sign of the trend; Case 3 (greatest consensus) occurs when >50% of model trends were statistically significant and >75% of the models agreed on the sign of the trend. We further evaluate whether past model trends have the same sign as observed trends.

Climate Modes and Decadal Variability

To examine how the trends in indices change over time, trends were evaluated over gradually decreasing the length of time prior to the present. Time series of large-scale climate modes were used to better understand the external factors driving natural variability in the extreme indices. The monthly North Atlantic Oscillation (NAO) data were downloaded from the NCAR/UCAR climate data guide at https://climatedataguide.ucar.edu/climate-data/hurrell-north-atlantic-oscillation-nao-index-pc-based (Hurrell et al. 2003). The monthly values for the winter season, December through February, were averaged and used in all calculations. The monthly Pacific Decadal Oscillation (PDO) was obtained from https://www.ncdc.noaa.gov/teleconnections/pdo/ (Mantua et al. 1997). The extended Multivariate ENSO index (MEI) was obtained from http://www.esrl.noaa.gov/psd/enso/mei/ (Wolter and Timlin 1998). The Atlantic Multidecadal Oscillation (AMO) was obtained from http://www.esrl.noaa.gov/psd/data/timeseries/AMO/

TABLE 3. The contemporary (1981–2010) climate normal for all climate extreme indices and a reference to the figure illustrating the time series.

Type	Index	Period	Figures	HadEX2	North	South
Cold	ID	Annual	S1, S2	28.7	6.8	3.0
Cold	FD	Annual	2, 3	114.7	80.9	63.1
Cold	TX10p	Annual		8.8	9.3	9.0
Cold	TX10p	DJF	4, 5		9.5	9.0
Cold	TX10p	MAM	4, 5		9.9	9.6
Cold	TX10p	JJA	4, 5		8.7	8.6
Cold	TX10p	SON	4, 5		8.7	8.6
Cold	TN10p	Annual		7.1	8.5	7.6
Cold	TN10p	DJF	S15, S16		8.7	7.9
Cold	TN10p	MAM	S15, S16		9.4	8.4
Cold	TN10p	JJA	S15, S16		7.6	7.3
Cold	TN10p	SON	S15, S16		8.2	7.3
Cold	TXn	Annual		−9.8	−6.6	−4.0
Cold	TXn	DJF	S9, S10		−5.8	−3.4
Cold	TXn	MAM	S9, S10		2.3	4.4
Cold	TXn	JJA	S9, S10		19.1	20.6
Cold	TXn	SON	S9, S10		5.8	7.4
Cold	TNn	Annual		−20.2	−16.7	−14.9
Cold	TNn	DJF	S13, S14		−15.9	−13.9
Cold	TNn	MAM	S13, S14		−7.9	−6.4
Cold	TNn	JJA	S13, S14		7.9	9.5
Cold	TNn	SON	S13, S14		−5.4	−4.5
Cold	CSDI	Annual	S1, S2	0.9	1.3	0.6
Warm	SU	Annual	S1, S2	96.4	128.1	141.6
Warm	TR	Annual	2, 3	19.6	40.0	53.9
Warm	GSL	Annual	2, 3	260.7	298.4	323.5
Warm	TX90p	Annual		11.2	11.2	11.0
Warm	TX90p	DJF	S11, S12		11.1	10.8
Warm	TX90p	MAM	S11, S12		11.6	11.5
Warm	TX90p	JJA	S11, S12		11.8	11.2
Warm	TX90p	SON	S11, S12		10.7	10.2
Warm	TN90p	Annual		11.3	10.8	11.2
Warm	TN90p	DJF	6, 7		10.3	10.5
Warm	TN90p	MAM	6, 7		10.3	11.1
Warm	TN90p	JJA	6, 7		11.5	12.1
Warm	TN90p	SON	6, 7		10.8	11.0
Warm	TXx	Annual		35.2	38.1	38.0
Warm	TXx	DJF	S17, S18		22.9	24.6
Warm	TXx	MAM	S17, S18		33.4	33.5
Warm	TXx	JJA	S17, S18		37.8	37.7
Warm	TXx	SON	S17, S18		33.2	33.7
Warm	TNx	Annual		23.2	26.9	26.9
Warm	TNx	DJF	S7, S8		12.4	14.7
Warm	TNx	MAM	S7, S8		20.5	21.0
Warm	TNx	JJA	S7, S8		26.3	26.7
Warm	TNx	SON	S7, S8		22.8	23.4
Warm	WSDI	Annual	S3, S4	4.6	4.4	3.2
Dry	CDD	Annual	S3, S4	18.5	22.4	22.0
Precip.	R10mm	Annual	8, 9	38.7	37.6	37.6
Precip.	R20mm	Annual	S5, S6	18.6	17.4	17.5
Precip.	Rx1day	Annual		78.9	112.9	121.2
Precip.	Rx1day	DJF	10, 11		48.7	49.8
Precip.	Rx1day	MAM	10, 11		58.5	56.0
Precip.	Rx1day	JJA	10, 11		74.1	81.2
Precip.	Rx1day	SON	10, 11		77.3	83.7
Precip.	Rx5day	Annual		116.6	168.6	173.2
Precip.	Rx5day	DJF	S19, S20		75.7	75.4
Precip.	Rx5day	MAM	S19, S20		92.1	88.6
Precip.	Rx5day	JJA	S19, S20		118.3	130.4

(continued)

TABLE 3. (continued)

Type	Index	Period	Figures	HadEX2	North	South
Precip.	Rx5day	SON	S19, S20		111.3	121.3
Precip.	SDII	Annual	S5, S6	12.1	12.0	12.4
Precip.	R95p	Annual	8, 9	272.9	259.5	264.6
Precip.	R99p	Annual	S5, S6	77.1	85.7	96.0
Precip.	PRCPTOT	Annual	8, 9	1,147.0	1,129.2	1,151.7
Precip.	CWD	Annual	S3, S4	5.1	6.0	6.1

Note: See Table 1 for index units.

(Enfield et al. 2001). The NAO, PDO, and AMO indices were filtered with a five-year moving mean to reduce short time-scale variability, and the MEI was left unfiltered to retain higher frequency El Niño Southern Oscillation (ENSO) variability. The R package corrplot (Wei 2021) was used to calculate the correlation between climate modes and the observed North and South extreme indices.

Water Quality Measurements

High-frequency (15 min) meteorological and water quality observations from shallow regions at Jug Bay, Maryland and Taskinas Creek, Virginia from the Chesapeake Bay National Estuarine Research Reserves (NERR) of Maryland and Virginia were used to relate atmospheric extreme event indices to in-water properties. These data are part of the NERR System-Wide Monitoring Program available through the Centralized Data Management Office (see http://cdmo.baruch.sc.edu). Atmospheric and water temperatures as well as oxygen concentration were collated and the data inspected. Eight short sections were identified as outliers and removed from the time series as a result of visual inspection.

RESULTS

Cold Event Annual Indices

All the annual cold event indices (see Table 1 for definitions) show a warming trend with reductions in the intensity of cold events significant in the North (TNn), decreases in the frequency of cold events significant in the North (icing days [ID], frost days [FD]; Figures S1c and 2a) and in both regions (TX10p, TN10p), and declines in the duration of cold events significant in the North (Cold Spell Duration Index [CSDI]; Figure S1e). Here, these trends are illustrated with the FD index, which is the annual count of days when the daily minimum temperature is <0°C (Table 1; Figures 2a and 3a). A larger decrease in FD is observed in the HADEx2 and North time series over the past century than for the southern region for which confidence is also lower (Table 4). There is high coherency between the North and South Chesapeake regions and the gridded HadEX2, indicating that weather patterns leading to FD variability tend to be broadly distributed over the Chesapeake Bay region with strong inter-annual variability. The mean number of FD using the 1981–2010 climate normal is 81 days for North Chesapeake, 63 days for South Chesapeake, and 115 days for the HadEX2 (Table 3). The larger number of FD in the HadEX2 gridded product is due to the inclusion of western weather stations at higher elevations.

The FD index declined by 6(2) days over the last century in the North(South) Chesapeake time series. These trends are generally strong enough to reach detection limits and are also modeled reasonably well. The FD trend for North Chesapeake and HadEX2 regions has Level 4 confidence (strong) (Table 4), though this trend is weaker and confidence (Level 3) is lower in the South. Similarly, the mean model ensemble over the past century has Level 4 confidence and Case 3 (stronger) consensus (Table 5).

The FD distributions from the 1951–1980 and 1981–2010 periods appear to be drawn from different distributions (p-value < 0.05) for North Chesapeake but are not significantly different for South Chesapeake (Figure 2b). Probability distributions, (Figure 2b), display a leftward shift, suggesting an increased probability of having fewer FD in the more recent period.

The mean of the climate model ensemble FD index also decreases over the past century (Table 5). In both future scenarios, FD declines throughout the 21st Century with the future model ensemble demonstrating Case 3 consensus (Figure 3a). The projected future trends (2006–2100) are −2(−5) days per decade for the RCP4.5(RCP8.5) scenarios (Table 5). There is little acceleration in the RCP4.5 FD future trend compared with the past, though an accelerated decline is projected for FD in the RCP8.5 scenario,

primarily after the model year 2050. Interannual variability in the future projections suggests that even in 2100, the number of FD could reach present-day levels in any given year. This is further illustrated in the PDFs of the present climate normal compared with the 2010–2040 climate normal model periods (Figure 3b). Model projections do not suggest a scenario where FD decline to zero over the next century in this region.

Seasonal Minimum Cold Temperature Patterns

Disaggregated by season, the indices representative of cool conditions generally shows warming (Table 4,

ID through CSDI). The trends in intensity, such as lowest daily minima and maxima (TNn, TXn) are less likely to be significant. A decrease in the percentage of days with low daily maxima and minima is significant in all seasons and regions (TX10p, TN10p; Figures 4 and S15). The TX10p index (percentage of days when the daily high temperature is below the 10th percentile) illustrates these patterns (Table 1; Figures 4 and 5). The number of cold days in the annual and seasonal indices declines in all the HadEX2, North, and South Chesapeake regions. Moderate coherence at the interannual time scale between the North and South Chesapeake regions suggests that the weather patterns governing seasonal low temperatures are coherent over the entire region.
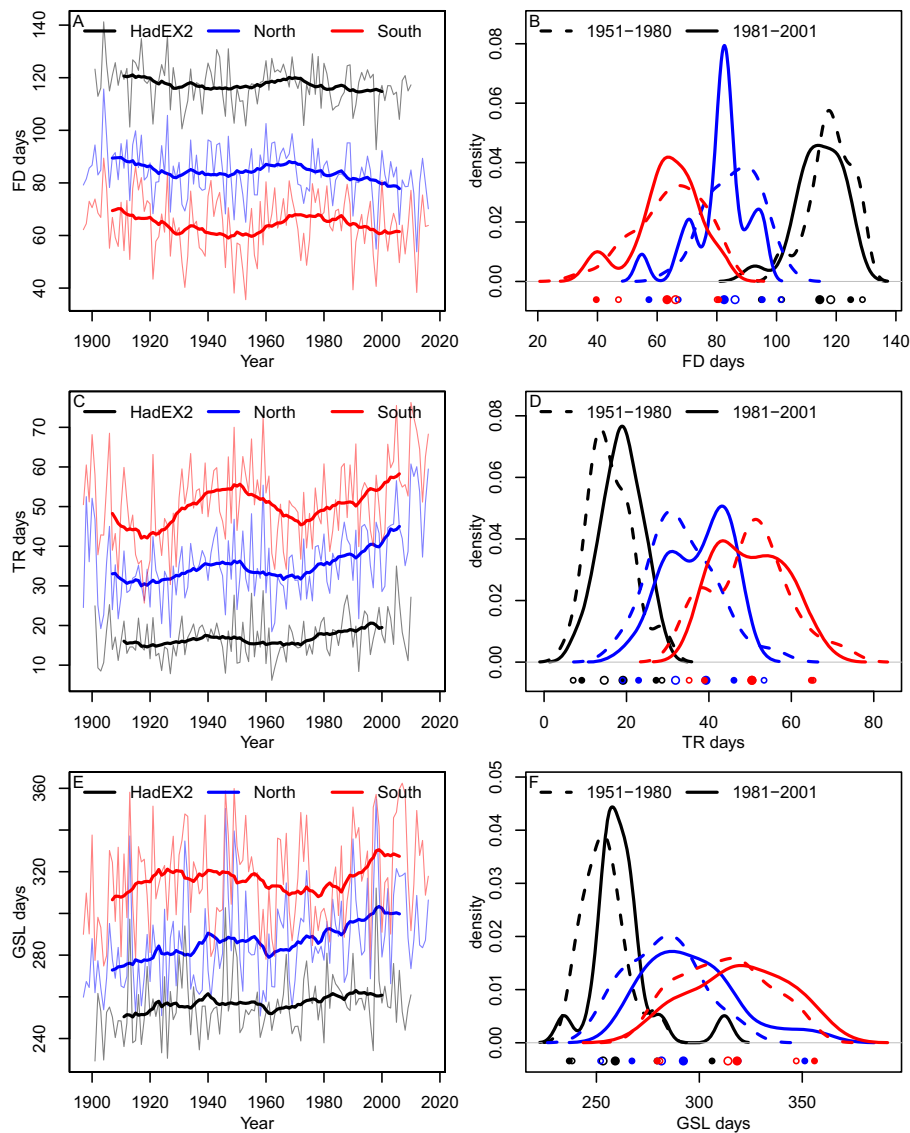

FIGURE 2. FD, TR, and GSL for HadEx2, North and South Chesapeake. (a, c, e) Unfiltered and 21-year running mean filtered time series. (b, d, f) Distributions for the 1951–1980 (dashed lines) and 1981–2010 climate normal (solid lines). 10th, 50th and 90th percentiles are shown as open circles for 1951–1980 and filled circles for 1981–2010.
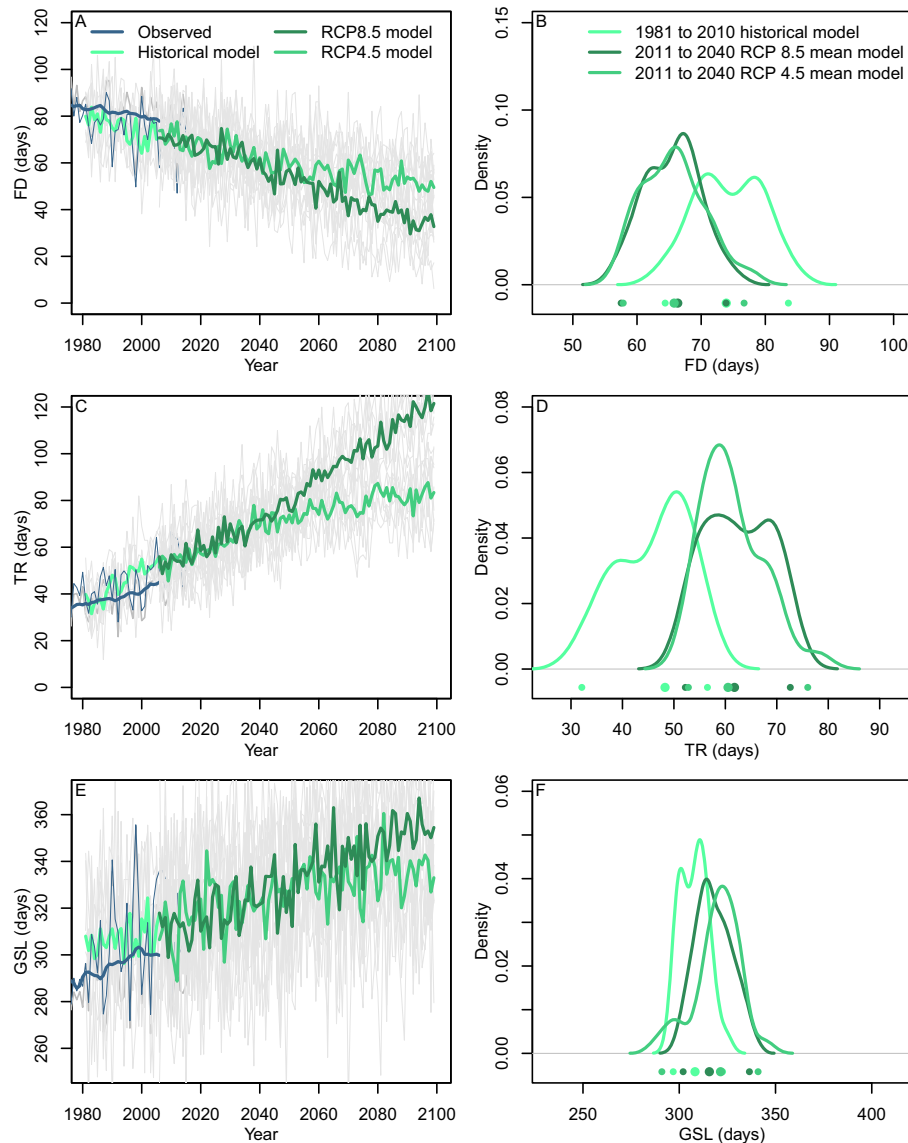
FIGURE 3. Observed and model FD, TR, and GSL. (a, c, e) North and South combined observations from 1981 to 2010 in blue with 21-year rolling means superimposed. In light gray are the individual models. The model ensemble mean for RCP4.5 or RCP8.5 is shown in light or dark green. (b, d, f) Distributions for the 1981–2010 period in light green, and 2011–2040 period RCP4.5 or RCP8.5 in light or dark green.

The long-term trend in this cold duration index TX10p (1895–2014) for the North(South) Chesapeake regions is significant in all seasons, with summer exhibiting the largest changes −122(−127) % declines over the past century based on the present-day climate normal, (Table 4). This is also simulated in the model ensemble which shows declining trends over the same time period with strong confidence (Level 4) and Case 3 consensus in all seasons (Figure 5; Table 5).

In the future projections, all seasons have fewer cool periods over the next century with high (Level 4) confidence and Case 3 consensus (Figure 5; Table 5), though summer reductions in cold events are projected to be weaker than other seasons in contrast to

the model trends over the past century. The future trend for the RCP8.5 scenario is of similar magnitude to the observed trends over the past century.

Warm Event Annual Indices

All the annual warm event indices (Table 1, summer days [SU] through Warm Spell Duration Index [WSDI]) have trends consistent with warming though the likelihood of significance is greater in the North Chesapeake. The intensity index for the highest annual daily minimum (TNx, Figure S7) is significant in both regions, but the highest annual daily maximum index (TXx) is not significant at the annual

TABLE 4. The decadal Sen's trend for all annual and seasonal indices.

Index	Period	HadEX2 (trend/decade)	North (trend/decade)	South (trend/decade)
ID	Annual	−0.43**	−0.16**	−0.04*
FD	Annual	−0.54**	−0.56**	−0.19*
TX10p	Annual	−0.28**	−0.68**	−0.45**
TX10p	DJF		−0.56**	−0.20**
TX10p	MAM		−0.59**	−0.49**
TX10p	JJA		−1.06**	−1.09**
TX10p	SON		−0.51**	−0.32**
TN10p	Annual	−0.43**	−0.51**	−0.31**
TN10p	DJF		−0.60**	−0.27**
TN10p	MAM		−0.42**	−0.48**
TN10p	JJA		−0.60**	−0.24**
TN10p	SON		−0.51**	−0.27**
TXn	Annual	0.06	−0.03	0.00
TXn	DJF		0.01	0.02
TXn	MAM		0.08**	0.10**
TXn	JJA		0.11**	0.16**
TXn	SON		0.15**	0.18**
TNn	Annual	0.16**	0.10**	−0.13
TNn	DJF		0.10*	−0.03
TNn	MAM		0.06**	0.05**
TNn	JJA		0.08**	0.05*
TNn	SON		0.17**	0.10**
CSDI	Annual	−0.13**	−0.38**	−0.02
SU	Annual	0.04	1.12**	0.99**
TR	Annual	0.46**	0.92**	0.83**
GSL	Annual	0.92**	2.31**	0.69**
TX90p	Annual	0.15	0.14**	−0.08
TX90p	DJF		0.27**	−0.05
TX90p	MAM		0.09**	0.09
TX90p	JJA		0.18**	014*
TX90p	SON		0.0	−0.15*
TN90p	Annual	0.29**	0.26**	0.08
TN90p	DJF		0.21**	−0.07
TN90p	MAM		0.25**	0.12*
TN90p	JJA		0.45**	0.29**
TN90p	SON		0.13**	0.05
TXx	Annual	−0.08**	0.02	0.01*
TXx	DJF		0.16**	0.11**
TXx	MAM		0.04*	0.01
TXx	JJA		0.02	0.02
TXx	SON		−0.03*	−0.03
TNx	Annual	0.02	0.14**	0.06**
TNx	DJF		0.13**	0.07**
TNx	MAM		0.16**	0.10**
TNx	JJA		0.13**	0.10**
TNx	SON		0.08**	0.05**
WSDI	Annual	0.10	0.17**	0.20**
CDD	Annual	−0.03	0.26**	0.03
R10mm	Annual	0.21**	−0.29**	−0.80**
R20mm	Annual	0.15**	0.06	−0.20**
Rx1day	Annual	0.63**	1.78**	3.01**
Rx1day	DJF		0.60**	0.24**
Rx1day	MAM		0.97**	0.66**
Rx1day	JJA		0.03	1.23**
Rx1day	SON		1.58**	2.32**
Rx5day	Annual	0.05	−0.54**	−1.85**
Rx5day	DJF		0.03	−1.43**

(continued)

TABLE 4. (continued)

Index	Period	HadEX2 (trend/decade)	North (trend/decade)	South (trend/decade)
Rx5day	MAM		0.23	−0.43
Rx5day	JJA		−0.69*	−1.44**
Rx5day	SON		1.13*	2.07**
SDII	Annual	0.07**	0.07**	0.04**
R95p	Annual	5.08**	8.63**	21.96**
R99p	Annual	2.24**	3.49**	9.69**
PRCPTOT	Annual	6.52**	−4.82**	−13.65**
CWD	Annual	0.00*	−0.57**	−0.93**

Note: Level of confidence is denoted as strong confidence (**), high confidence (*), or low confidence (no *). See Table 1 for units.

time scale in either region. Increases occur in the frequency of warm events (SU, tropical nights [TR], and in the North only, percentage of days with highs greater than the 90th percentile (TX90p), and lows greater than the 90th percentile (TN90p); Figures S1a and 2c). Increases occur in the duration of warm events (WSDI; Figure S3a). Here, this pattern is illustrated with the TR index (annual count of days when the daily minimum temperature >20°C) which is a frequency index for nighttime high temperatures (Figure 2c; Table 1). The variability in the TR time series generally has high coherence across the region, particularly for major events. The 1981–2010 climate normal TR is 40.0, 53.9, and 19.6 days in the North Chesapeake, South Chesapeake, and HadEX2 time series, respectively (Table 3).

The TR long-term trend has strong confidence (Level 4) for all three of the time series (Table 4). An increase of 9, 8, and 5 days occurs in TR from 1905 to 2005 in North Chesapeake, South Chesapeake, and HadEX2 time series, respectively. Past trends in the model ensemble TR (Figure 3c) are positive with Level 4 confidence and Case 3 consensus (Table 5). However, the model ensemble trend over the past century is greater than the observational record.

An Anderson–Darling test for observed TR from the 1951 to 1980 and 1981 to 2010 reference periods is significantly different for the North but not the South Chesapeake time series and displays a rightward shift (higher likelihood of annual TR events) (Figure 2d).

The increase in TR continues in the future projections (Case 3 consensus). Trends (2006–2100) are projected to be 4(8) days per decade for the RCP4.5 (RCP8.5) scenarios (Table 5). An accelerated trend is projected for the RCP8.5 scenario which is primarily evident after 2050 (Figure 3c). Between 2009 and 2025, TR increases by 6(13) days in the RCP4.5 (RCP8.5) scenarios and between 2009 and 2050 by 15

TABLE 5. The 21-year moving average decadal Sen's trend for all model-derived indices. Past trends are calculated as 1900–2015, future trends are calculated as 2006–2100.

Index	Period	Past	Future RCP4.5	Future RCP8.5
ID	Annual	−1.54**	−0.71**	−1.22**
FD	Annual	−3.64**	−2.19**	−4.64**
TX10p	DJF	−0.22**+	−0.52**	−0.87**
TX10p	MAM	−0.67**	−0.5**	−0.79**
TX10p	JJA	−0.7**	−0.37**	−0.53**
TX10p	SON	−0.36**	−0.49**	−0.72**
TN10p	DJF	−0.24**+	−0.64**	−0.73**
TN10p	MAM	−0.65**	−0.5**	−0.63**
TN10p	JJA	−0.61**	−0.46**	−0.47**
TN10p	SON	−0.55**	−0.49**	−0.63**
TXn	DJF	0.17**	0.3**	0.58**
TXn	MAM	0.11**	0.28**	0.62**
TXn	JJA	0.15**	0.26**	0.63**
TXn	SON	0.09**	0.29**	0.62**
TNn	DJF	0.19**	0.32**	0.68**
TNn	MAM	0.11**	0.28**	0.54**
TNn	JJA	0.12**	0.28**	0.72**
TNn	SON	0.1**	0.33**	0.65**
SU	Annual	7.05**	2.97**	7.02**
TR	Annual	6.53**	3.55**	8.03**
GSL	Annual	2.79**	2.67**	5.47**
TX90p	DJF	0.24**	1.15**	1.46**
TX90p	MAM	0.51**	2.3**	5.46**
TX90p	JJA	0.57**	3.11**	7.87**
TX90p	SON	0.56**	1.47**	3.87**
TN90p	DJF	0.3**	0.85**	1.28**
TN90p	MAM	0.63**	2.04**	5.03**
TN90p	JJA	0.85**	3.83**	8.09**
TN90p	SON	0.33**	0.85**	2.77
TXx	DJF	0.08**	0.16**	0.41**
TXx	MAM	0.09**	0.27**	0.64**
TXx	JJA	0.09**	0.29**	0.74**
TXx	SON	0.07	0.26**	0.76**
TNx	DJF	0.09**	0.22**	0.5**
TNx	MAM	0.1**	0.24**	0.56**
TNx	JJA	0.08**	0.27**	0.62**
TNx	SON	0.08**	0.25**	0.64**
WSDI	Annual	4.52**	3.95**	15.77**
CDD	Annual	0.52**	0.08**	0.27**
R10mm	Annual	0.58**	0.19**+	0.08**+
R20mm	Annual	0.1	0.21**	0.27**+
Rx1day	DJF	0+	0.51**	1.2**
Rx1day	MAM	−0.04+	0.21	1.02**
Rx1day	JJA	0.33	0.37	0.44+
Rx1day	SON	0.01+	0.14+	0.57**+
Rx5day	DJF	0.14+	0.84**	1.37**
Rx5day	MAM	0.07+	1.13**	1.69**
Rx5day	JJA	0.62	0.85**+	1.14**
Rx5day	SON	−0.12+	0.88**	0.47**+
SDII	Annual	0.17**	0.09**	0.13**
R95p	Annual	20.24**	12.55**	19.7**
R99p	Annual	16.82**	8.15**	13.56**
PRCPTOT	Annual	13.91**	13.37**+	12.72**
CWD	Annual	−0.03	0.1**+	0+

Note: A significant trend significance is denoted as **. Case 1 and Case 2 consensus (weaker consistency between models) is indicated with the (+) symbol, and Case 3 consensus (stronger consistency between models) is indicated with no symbol. See Table 1 for units.

(33) days (Table 5). All of the model simulations demonstrate a rightward shift to a higher probability of TR in the probability distributions (Figure 3d), with an indication of narrower distributions suggesting decreased interannual variability.

Seasonal Maximum Warm Event Patterns

On a seasonal basis, warm events have also increased. The number of warm events expressed as the percentage of days where the daily maximum and minimum temperatures exceeded the 90th percentile (TX90p, TN90p; Figures S11 and 6) increased in the North Chesapeake in all seasons except Fall TX90p. However, the South Chesapeake only has statistically significant increases in summer TN90p. Similarly, the highest seasonal daily temperature maximum increases significantly only in winter (TXx; Figure S17) in both regions. The trend is significant over all regions and seasons for the highest nighttime daily minimum temperatures (TNx; Figure S7). This pattern is illustrated using TN90p which counts the number of daily lows higher than the 90th percentile of daily lows in the climate normal (Table 1). Observed increases in warm event count are generally smaller than for the equivalent cold-temperature seasonal indices (Table 4; Figure 6). The model ensemble also has modest increasing trends over the past century in all seasons, slightly higher in spring and summer (Figure 7; Table 5).

The percentage of days with high daily minimum temperatures (TN90p; Figure 6) increases by 20% (winter), 24% (spring), 39% (summer), and 12% (fall) between 1905 and 2005 in the North Chesapeake regions. Increases are 24% (summer) in the South Chesapeake.

Future model ensemble increases are projected to be higher in spring and summer, though all trends have strong confidence (Level 4) with Case 3 consensus. While this pattern is not as strong in the past observations, the magnitude of the model and observed trends are broadly comparable. The two model scenarios begin to diverge mid-century, except for winter which has a similar trend in both scenarios.

Duration Event Indices

The duration-based Growing Season Length (GSL) index is defined as the period in which wheat can germinate and flourish (Figure 2e; Table 1). The range of interannual GSL variability across the region is considerable with year-to-year variations of as much as 100 days in both the North and South Chesapeake (Figure 2e). The 1981–2010 climate
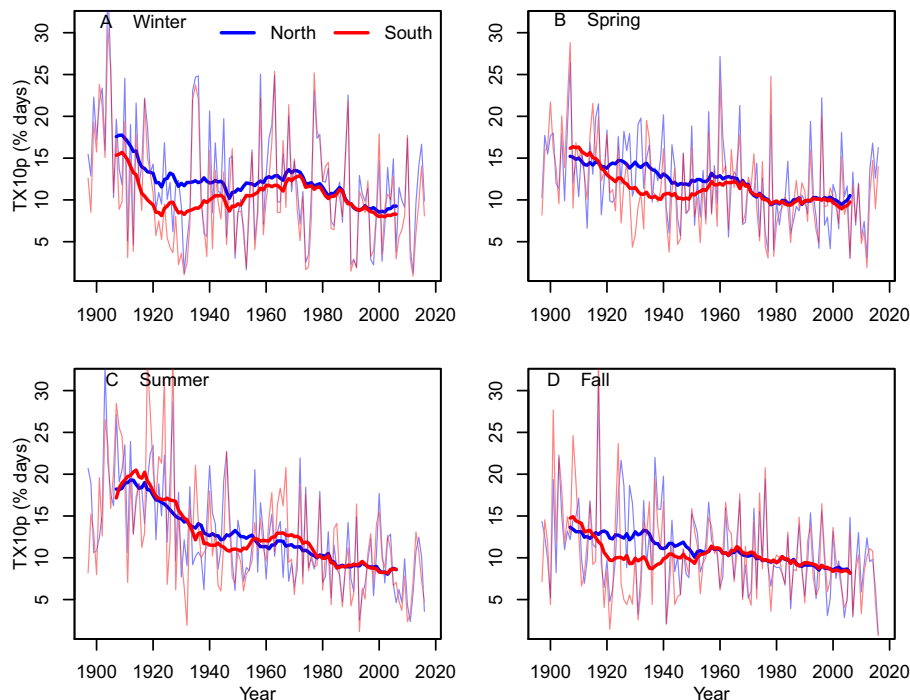
FIGURE 4. TX10p aggregated as North and South Chesapeake and by season. Heavy lines show the 21-year rolling mean filtered time series. (a) Winter, (b) Spring, (c) Summer, (d) Fall.

normal GSL is 298, 324, and 261 days in the North, South, and HadEX2 regions, respectively (Table 3).

The significant increase in GSL has strong confidence (Level 4; Table 4). The model ensemble is also significantly increasing with a similar magnitude of change over the past century compared with observations (Table 5; Figure 3e). GSL increases by 23(7) days between 1905 and 2005 in the North(South) Chesapeake time series (Table 4).

This increase in GSL continues in both future scenarios with strong confidence (Level 4) and high consensus (Case 3), with little difference in the means of the model ensembles until the mid-21st Century. Future trends (2006–2100; Figure 3g) are projected to be 3(5) days per decade for the RCP4.5(RCP8.5) scenario, respectively (Table 5). Between 2009 and 2025, GSL is projected to increase by 4.3(8.8) days in the RCP4.5(RCP8.5) scenario, and between 2009 and 2050 GSL increases by 10.9(22) days. The variance in GSL increases with time in the models (Figure 3f). Growing seasons as short as the minimum observed in the 1981–2010 climate normal continue to occur over the next century in the model ensemble.

Precipitation Event Annual Indices

Precipitation indices are highly variable and show generally less spatial coherence in variance between the North and South Chesapeake regions (Table 1, Consecutive Dry Days through Consecutive Wet Days [CWD]). However, a consistent pattern emerges of increased short-term precipitation intensity in both the North and South Chesapeake regions as measured by the annual sum of precipitation occurring in events greater than the fifth and first percentile (R95p, R99p; Figures 8c and S5e) with small declines in annual precipitation in both regions (PRCPTOT; Figure 8e), and declines in the number of days with precipitation delivered in light rainfall events (R10mm, R20mm; Figures 8a and S5c) (Table 1). This leads to a significant reduction in CWD in the North (Figure S3e), and a small increase in the daily rainfall intensity (SDII; Figure S5a) in both regions. Here we illustrate these changes with three precipitation indices, R10mm which describes the number of days with precipitation above 10 mm (Figure 8a), R95p which describes the annual sum of precipitation that occurs in events exceeding the 95th percentile (Figure 8c), and PRCPTOT, the annual total precipitation amount (Figure 8e). More than one station reports likely anomalous maxima at the start of the record for R10mm and PRCPTOT in the Southern Chesapeake, however, as these occur across two or more stations, they have been retained, and these do not project strongly onto the 21-year averaged time series. R10mm climate normals are 37.6(37.6) days in the North(South) (Table 3). R95p contemporary
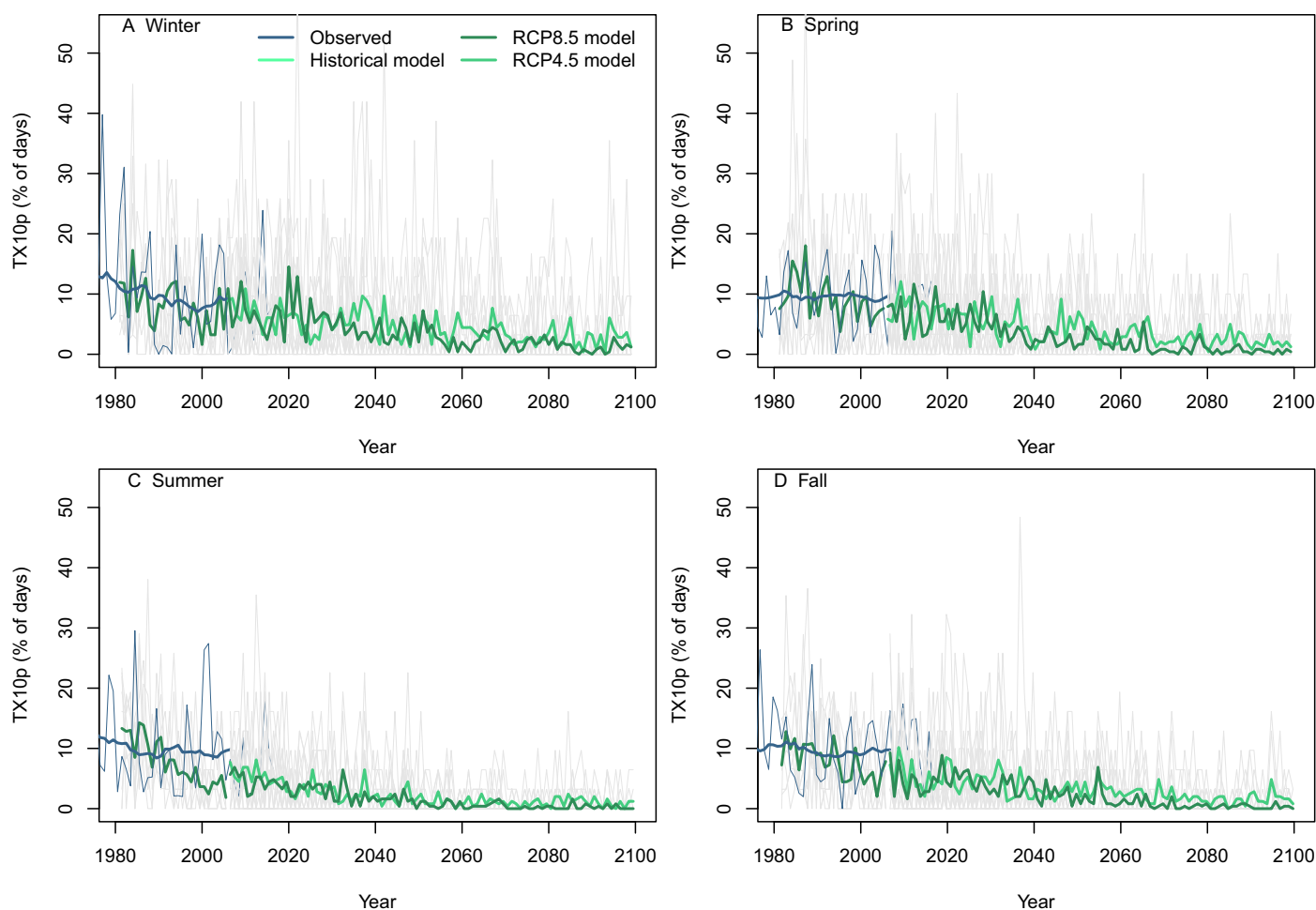
FIGURE 5. Future TX10p. North and South combined observations from 1981 to 2010 in blue, with the 21-year rolling means superimposed. In light gray are the individual model projections and the mean of the model ensemble for the present and RCP4.5 or RCP8.5 scenario is shown in light or dark green. (a) Winter, (b) Spring, (c) Summer, (d) Fall.

climate normal means are 259.5(264.6) mm in the North(South), displaying no strong regional differences (Table 3). PRCPTOT climate normal means are 1,129.2(1,151.7) mm in the North(South), with little regional difference.

The long-term trends in R10mm are negative, with 8(21) % declines over the past century in the North (South) regions. R95p increases for North/South Chesapeake regions by 33(83) % with strong confidence (Table 4). PRCPTOT shows small declines over the century of 4(12) % in North(South) Chesapeake regions. Past trends in the model ensemble (Figure 9; Table 5) differ from observations, with positive trends in R10mm, positive and realistic magnitudes of change in R95p, and a projected increase in PRCPTOT. The models thus do not reproduce the past century trends well except for R95p.

The increase in R95p already observed over the Chesapeake Bay continues in the future projections with a similar slope to the past model mean (Level 4

strong confidence and Case 3 consensus, Table 5). An accelerated trend is projected for the RCP8.5 scenario with the acceleration primarily evident after 2050. Between 2009 and 2025, R95p increases by 20.1(31.5) mm per year in the RCP4.5(RCP8.5) scenarios, respectively, and between 2009 and 2050 by 51.5 (80.8) mm per year. All of the model simulations indicate a rightward shift to higher R95p values in the probability distributions (Figure 9e), though distributions do not widen (little to no change in variability). Projected changes in the R10mm and PRCPTOT indices are modest and highly variable, but also highly uncertain based on the model's inability to reproduce past century trends.

Seasonal Precipitation Intensity Patterns. Measures of seasonal precipitation intensity include a one-day measure of maximum daily precipitation intensity (Rx1day; Table 4; Figure 10). This index has a generally increasing trend, with only the
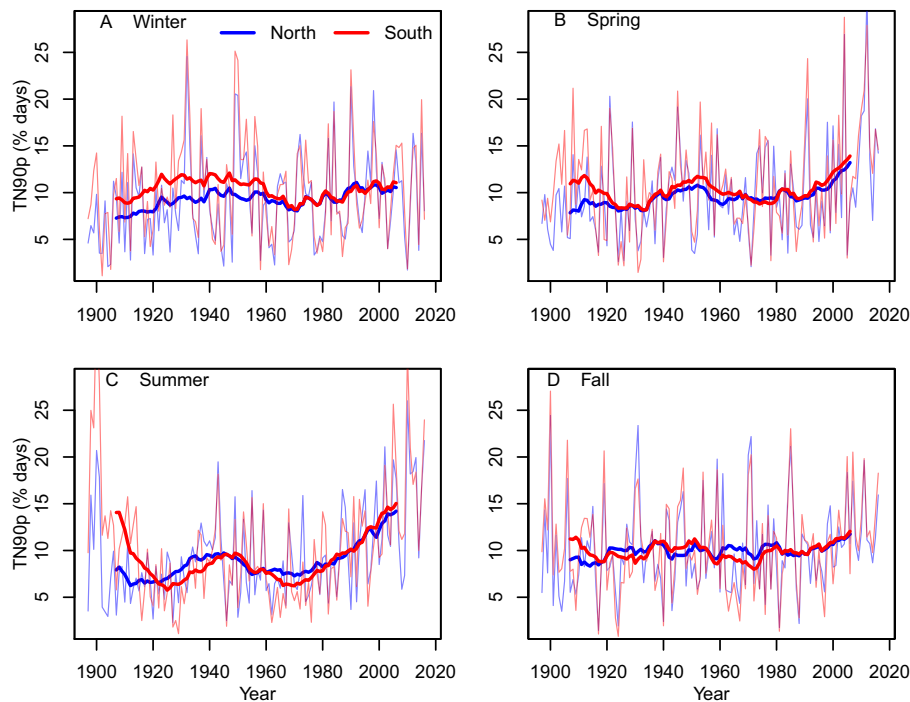
FIGURE 6. TN90p aggregated as North and South Chesapeake and by season. Heavy lines show the 21-year rolling mean filtered time series. (a) Winter, (b) Spring, (c) Summer, (d) Fall.

summer North trend insignificant. The other seasonal measure of precipitation intensity reflects longer time scales (Rx5day; Figure S19) and is more variable, with a declining trend significant in the South Chesapeake in winter and summer. Model ensemble trends over the past century are small and variable with low significance (Figure 11).

Spring rainfall maxima increase in the North Chesapeake over the past century by 15%, summer rainfall in the South Chesapeake by 31%, and fall rainfall maxima increase by 20% and 32% in North and South Chesapeake, respectively, over the past century.

The future model ensemble shows increasing trends in Rx1day in all seasons except spring consistent with past trends in observed Rx1day, but these are not significant (Figure 11; Table 5). The future model ensemble increases in Rx1day are highest in winter and spring with strong confidence (Level 4) and Case 3 consensus for the RCP8.5 scenario (Tables 4 and 5). Rx1day is projected to increase by 0.8(1.9) mm (2009–2025) in winter in the RCP4.5 (RCP8.5) scenarios, respectively, and winter Rx1day increases by 2.1(4.9) mm (2009–2050). Spring Rx1day increases by 0.3(1.6) mm (2009 and 2025), and by 0.9 (4.2) mm (2009 and 2050) for the two scenarios. Summer Rx1day increases by 0.6(0.7) mm (2009–2025), and by 1.5(1.8) mm (2009–2050). Fall Rx1day increases by 0.2(0.9) mm (2009–2025) and by 0.6(2.3)

mm (2009–2050) in the RCP 4.5(8.5) scenarios. The two model scenarios show little divergence over the next century, though confidence is generally higher in the tendency for the RCP8.5 scenario.

To better understand how much variance in the indices can be explained by large-scale climate patterns, we cross-correlate all the indices with the NAO, AMO, PDO, and MEI, though only indices with significant correlations are shown (Figure 12). For comparison, we also correlate the mean annual or mean seasonal temperature (T_{mean}) and precipitation (P_{mean}) with the climate mode time series.

On an annual basis, only FD, GSL and mean temperature (FD, GSL, and T_{mean}) are correlated with the NAO (Figure 12a). The ENSO index, MEI, is positively correlated with the highest annual temperatures (TXx), and negatively correlated with the percentage of cold days (TX10p). The PDO is positively correlated with many cold events measures such as FD, ID, and percentage of time experiencing anomalously cold events (FD, ID, and TN10p), and negatively correlated with measures of heat such as increases in the percentage of time experiencing warm events, GSL, annual minimum temperature and mean temperature (TN90p, GSL, TNn, and T_{mean}). The PDO is also negatively correlated with precipitation intensity (R99p). The AMO is negatively correlated with annual cold measures (ID, FD, TX10p, TN10p), and has stronger positive
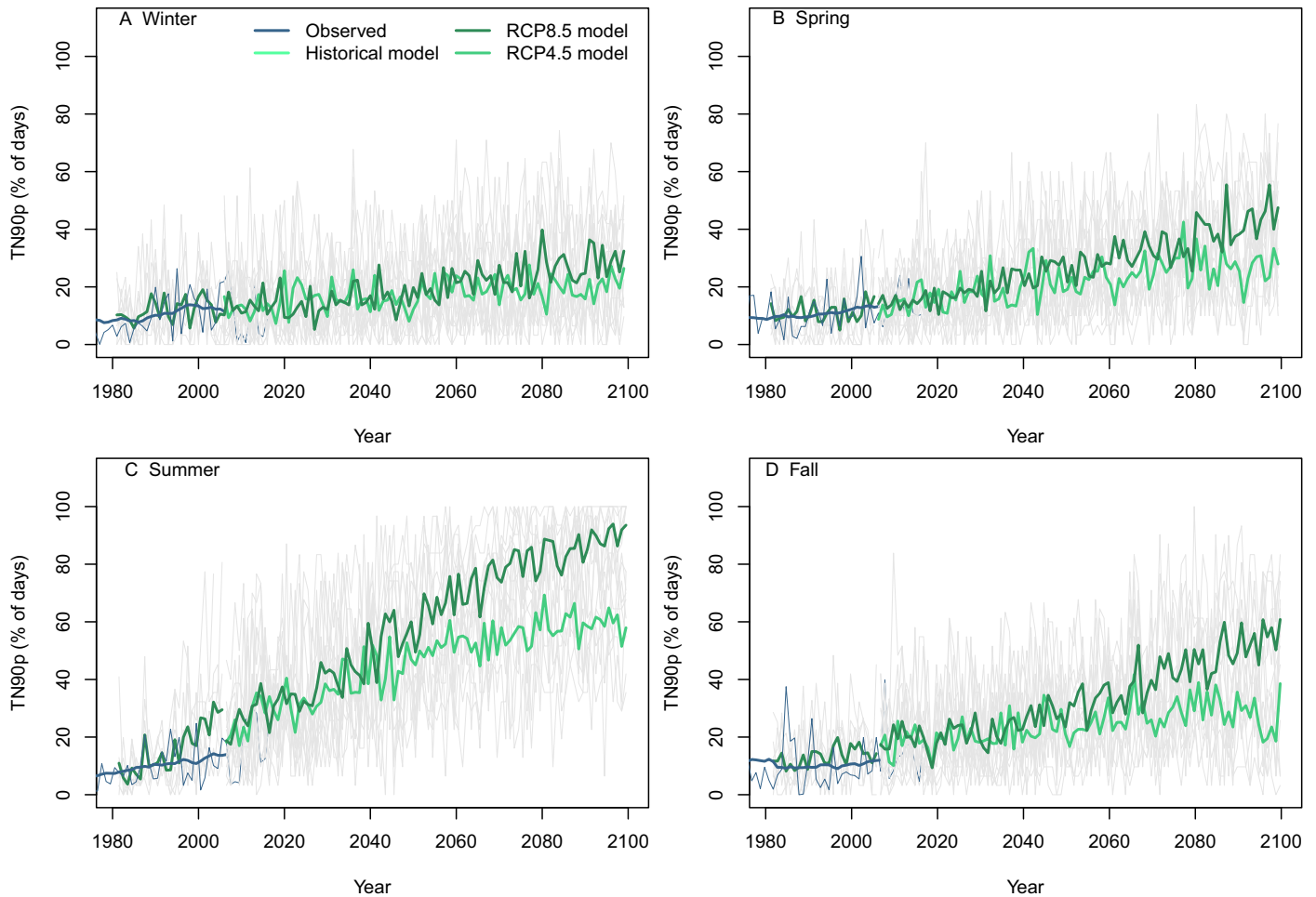
FIGURE 7. Future TN90p. North and South combined observations from 1981 to 2010 in blue, with the 21-year rolling means superimposed. In light gray are the individual model projections and the mean of the model ensemble for the present and RCP4.5 or RCP8.5 scenario is shown in light or dark green. (a) Winter, (b) Spring, (c) Summer, (d) Fall.

correlations with warm day frequencies (SU, TR, TXx, TX90p, TN90p). High AMO is also positively correlated with elevated precipitation intensity (Rx1-day, SDII, R99p).

The NAO wintertime index has stronger correlations with winter extreme climate indices. Positive phases are associated with increased high temperatures (TXx, TNx, T_{mean}), frequency of warm days and nights (TX90p, TN90p) and moderately decreased frequency of low temperatures (TX10p) (Figure 12b). No significant relationships are found between NAO and the precipitation indices in winter. ENSO (MEI) is positively associated with winter precipitation intensity (Rx1day), and negatively associated with winter warm event intensity and duration (TXx, TX90p), but is also uncorrelated with averaged temperature or precipitation. Winter PDO influence is strongly expressed in winter indices, negatively correlated with measures of warming, and positively correlated with measures of cooling. Duration indices are more

highly correlated than intensity indices. The AMO has positive correlations with increasing winter daily minimum temperatures (TXn, TNn) and a negative relationship with the duration of coldest annual temperatures (TN10p).

In summer, the pattern for NAO changes, with a positive phase leading to a slightly reduced count and intensity of warm events in summer (TX90p, TNn, Figure 12c). Positive ENSO contributes to a reduction in intense and mean precipitation in summer (Rx1day, Rx5day, P_{mean}), whereas PDO, which had no winter impact on precipitation, is also negatively correlated with summer precipitation intensity. A positive AMO is also strongly correlated with summertime high temperatures, particularly with more prolonged warm spells, and reduced duration of cold events. In summer and fall (not shown), the AMO index is also significantly positively correlated with precipitation indices.

The ecological and/or water quality implications of these events may also depend on their covariance, so
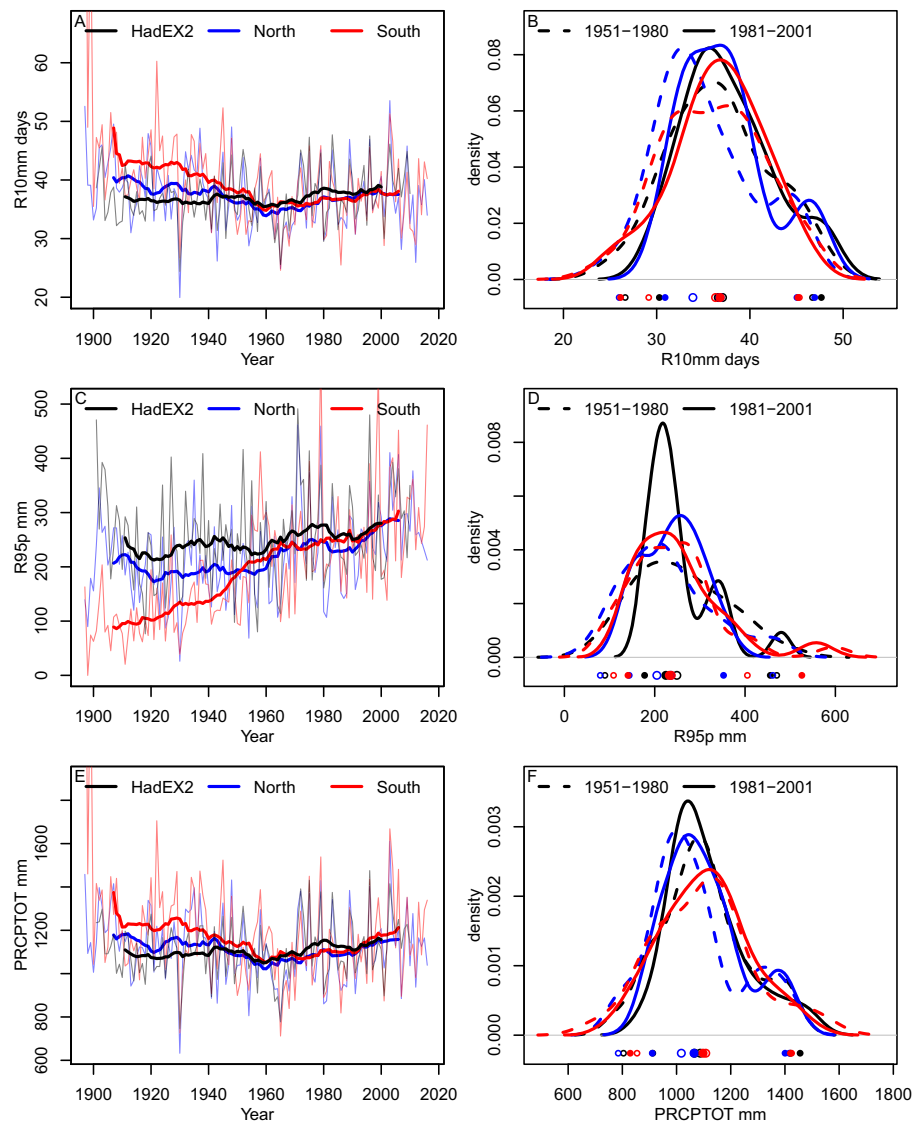
FIGURE 8. R10mm, R95p, and PRCPTOT for HadEx2, North and South Chesapeake. (a, c, e) Unfiltered and 21-year running mean filtered time series. (b, d, f) Distributions for the 1951–1980 (dashed lines) and 1981–2010 climate normal (solid lines). 10th, 50th, and 90th percentiles are shown as open circles for 1951–1980 and filled circles for 1981–2010.

we cross-correlated precipitation indices with thermal indices. On an annual basis (Figure 12a), intense precipitation (R99p) increased with decreases in the duration of cold events (TX10p, TN10p) and with increases in the duration of nighttime warm events (TR, TN90p). However, increased total annual precipitation was nearly oppositely associated with reduced daily temperature maxima and warm event duration (TXx, TX90p) and increased duration of cold events (TX10p). Winter precipitation indices were not correlated with temperature events suggesting that the patterns observed on an annual basis are likely driven by spring (not shown) and summer. Indeed, the indices associated with summer high rainfall events (Rx1day, Rx5day) were correlated negatively with

cold event duration (TN10p) and positively with warm event duration and temperature intensity (TN90p, TNn).

DISCUSSION

Which Indices Show Centennial Scale Trends?

The examples presented here mostly illustrate climate extreme indices that demonstrate significant change over the past century. The overall pattern is summarized in Figure 13, though in some cases
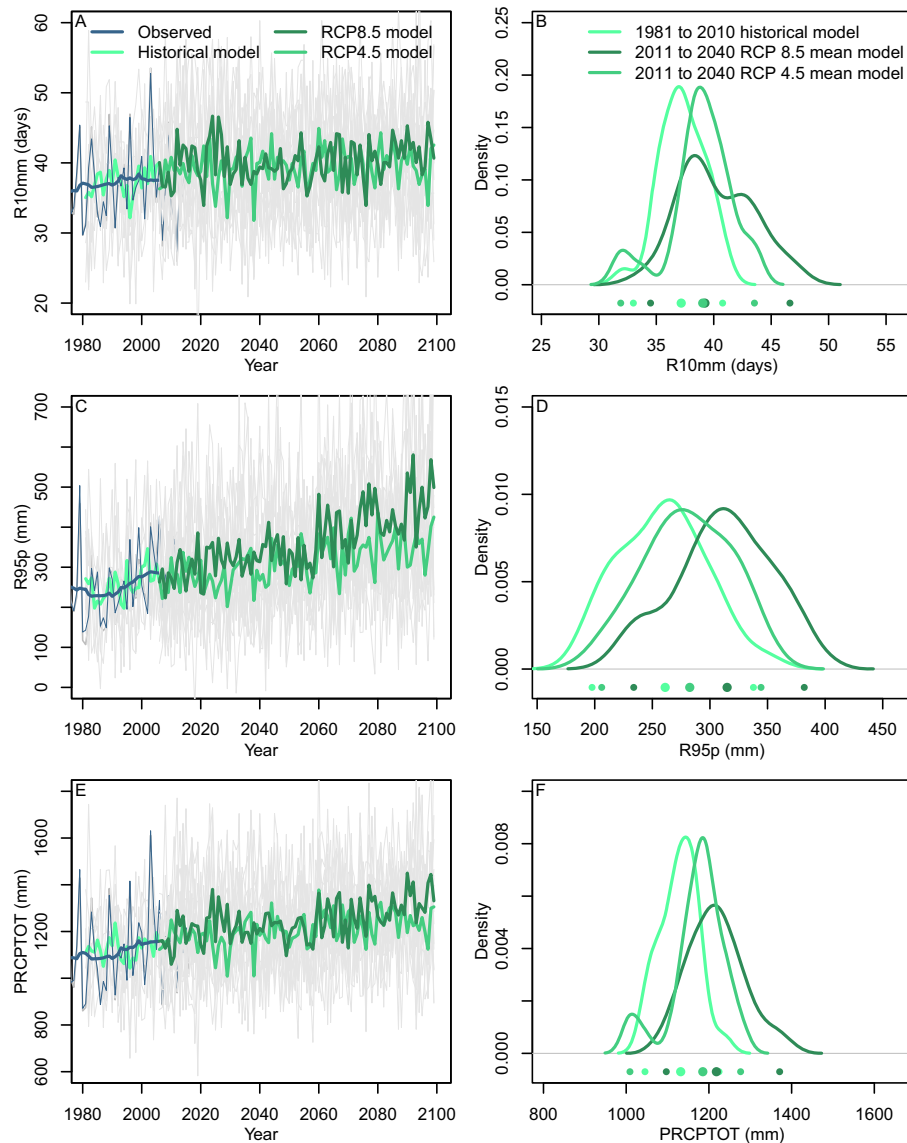
FIGURE 9. Future R10mm, R95p, and PRCPTOT. (a, c, e) North and South combined observations from 1981 to 2010 in blue with 21-year rolling means superimposed. In light gray are the individual models. The model ensemble mean for RCP4.5 or RCP8.5 is shown in light or dark green. (b, d, f) Distributions for the 1981–2010 period in light green, and 2011–2040 period RCP4.5 or RCP8.5 in light or dark green.

percentage changes have different confidence measures than the absolute trends. However, a number of measures do not show major change over the observational record. This is due to the large variance that obscures significant trend detection, insensitivity of the local region to the index, or to apparent stability of the local climate system for the given index. For example, while the collective indices generally show reductions in cold events, FD and ID are decreasing only slightly in the North, and are not significantly changing in the South Chesapeake (Figure 13). These are threshold indices, thus it is unsurprising that a warmer region would have few overall FD or ID and change in a small quantity

might be insignificant. Neither region has seen a significant change in the annual or wintertime coldest daily minimum or daily maximum temperatures (TNn, TNx). These thresholds are important for defining the ecological range for species with lower cold tolerances which may indicate that the habitat suitability of these regions is not expanding to accommodate warmer climate species with hard freezing thresholds.

Similarly, for warm events, there are general increases reflecting a warmer overall climate, though some indices stand out as changing little if at all. Only in winter did the absolute maximum temperature (TXx) increase slightly in the North and South.
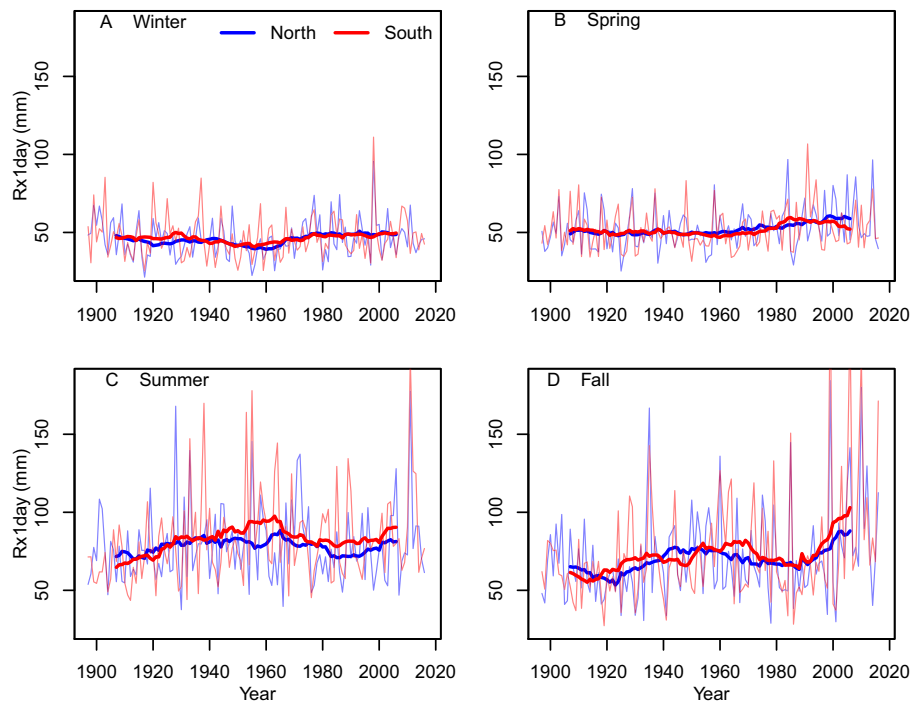
FIGURE 10. Rx1day aggregated as North and South Chesapeake and by season. Heavy lines show the 21-year rolling mean filtered time series. (a) Winter, (b) Spring, (c) Summer, (d) Fall.

In the South Chesapeake, there is no change in the percentage of time spent in abnormally high daily high temperature (TX90p) conditions.

While there are significant increases in annual measures of rainfall intensity, the patterns are mixed and not regionally coherent in the seasonal data. The maximum daily rainfall amount (Rx1day) did not change significantly in the North in summer. The five-day maximum rainfall amount (Rx5day) decreased annually and in winter and summer in the south. These inconsistent patterns are somewhat in line with the recent regional climate assessment (Easterling et al. 2017) with the North and South regions reflecting the larger regional patterns. However, at the scale of the Chesapeake Bay (~300 km along the main stem), trends in climate extreme indices vary between the Northern and Southern Bay. Trends in rainfall amount and intensity remain generally challenging to interpret over the region.

Confidence in Future Projections

To evaluate model projections of future climate, quantitative measures of how well the models perform over the historical record are needed. Here, we use measures of trend agreement between models (consensus) as well as whether the mean model trend has the same sign and magnitude as the observed trend over the past century (Table 5). In general, changes in cold events are well represented in the model ensemble. The model mean overpredicts past changes in FD and ID, though consensus between the models is high.

Similarly, warm events trends are captured by the models over the past century, though the model ensemble overpredicts increases in SU and TR. Neither models nor data show a large trend in the maximum temperatures experienced in a season, though both show increases in the highest daily minimum temperatures (TNx), which suggest a general increasing trend of nighttime temperatures. This is consistent with observed large scale patterns (Karl et al. 1993; Wang et al. 2016), and has been attributed in part to changes in precipitable water vapor that led to more reflection of solar radiation during the day while trapping long wave radiation at night (Dai et al. 1999).

In general, the local trends over the past century in precipitation indices are poorly simulated by models. Either the model trends are insignificant (e.g., Rx1day), or the model trend is simply wrong (PRCPTOT). However, even in observations, the trends in precipitation are weaker and embedded within high interannual variability, making them more challenging to detect. The model ensemble has higher skill at predicting increases in the amount of rainfall delivered in extreme events (R95p, R99p,
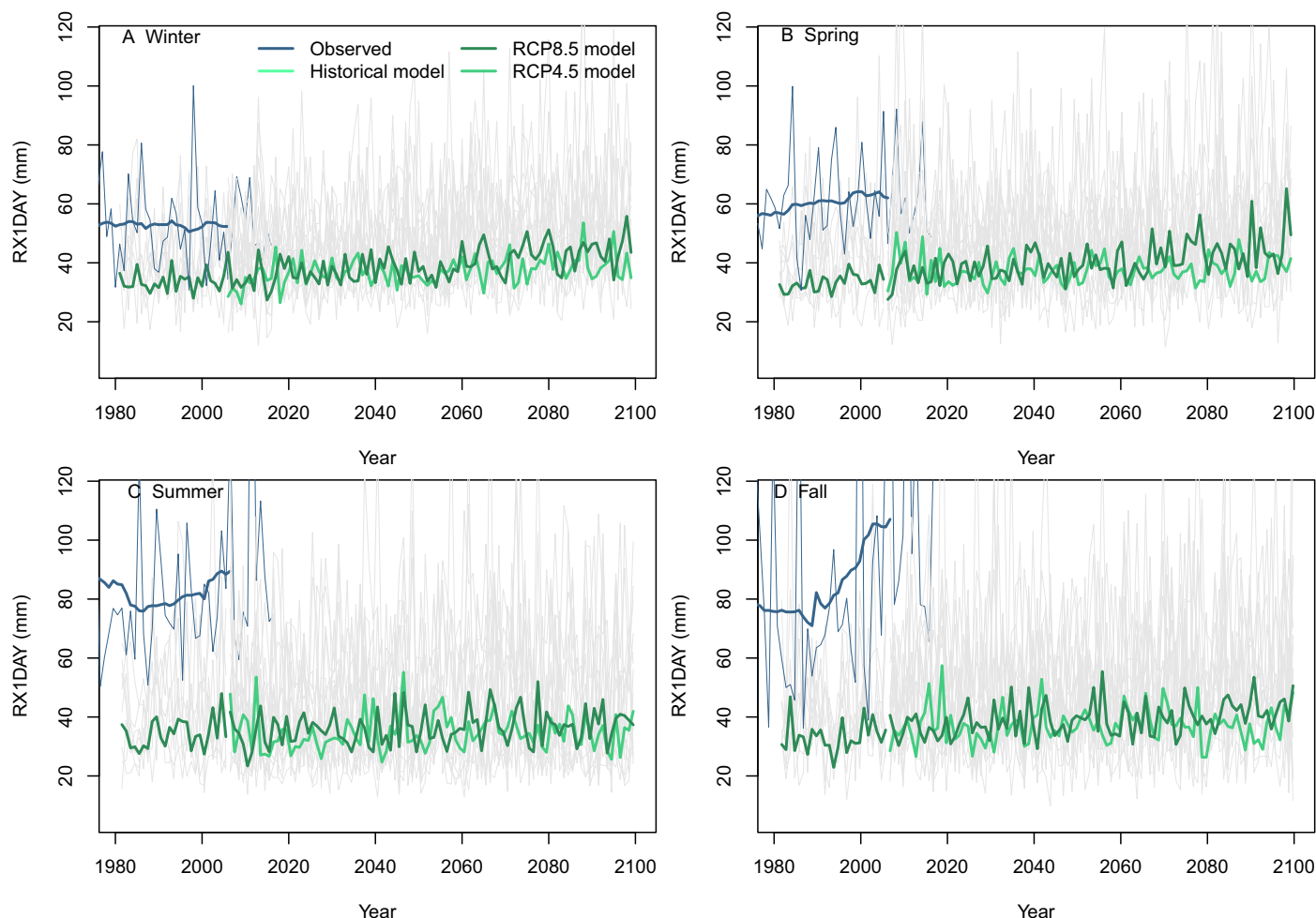
FIGURE 11. Future Rx1day. North and South combined observations from 1981 to 2010 in blue, with the 21-year rolling means superimposed. In light gray are the individual model projections and the mean of the model ensemble for the present and RCP4.5 or RCP8.5 scenario is shown in light or dark green. (a) Winter, (b) Spring, (c) Summer, (d) Fall.

CWD), suggesting that increases in atmospheric temperature are translated to more extreme precipitation in general.

Downscaled climate projections, using either statistical relationships or regional climate models, may be able to better back predict the past century than these global climate models. However, underlying errors in the models cannot be simply adjusted, and may require improvements to model physics and resolution. Downscaling or bias correction approaches can alter the trends in the model simulations (Maraun et al. 2017). As a result, we have not used downscaling approaches aside from annual mean correction, which will not alter the reported trends.

Comparison with Prior Local and Regional Studies

A number of previous studies provide insights into expected future regional climate changes (Peterson et al. 2001; Pyke et al. 2008; Karl et al. 2009; Najjar et al. 2010; IPCC 2014; Melillo et al. 2014; Easterling et al. 2017; Vose et al. 2017). In general, atmospheric warming is expected to increase over the next century, mirrored in the shallow water environments of Chesapeake Bay with water temperature increases projected from 2°C to 6°C (Pyke et al. 2008; Najjar et al. 2010). This warming projection varies between the Northeast and Southeast U.S., with more warm spells expected in the Northeast and more warm nights and fewer cold days expected in the Southeast (Carter et al. 2014; Horton et al. ; Melillo et al. 2014). However, organisms and processes in the Chesapeake Bay estuary may be more sensitive to summertime maximum temperatures or the duration of the coldest wintertime freeze, neither of which is reflected in the average annual temperature.

Many regional studies on past and future climate changes encompass the Chesapeake Bay region (Brown et al. 2010; Kunkel, Stevens, Stevens, Sun,
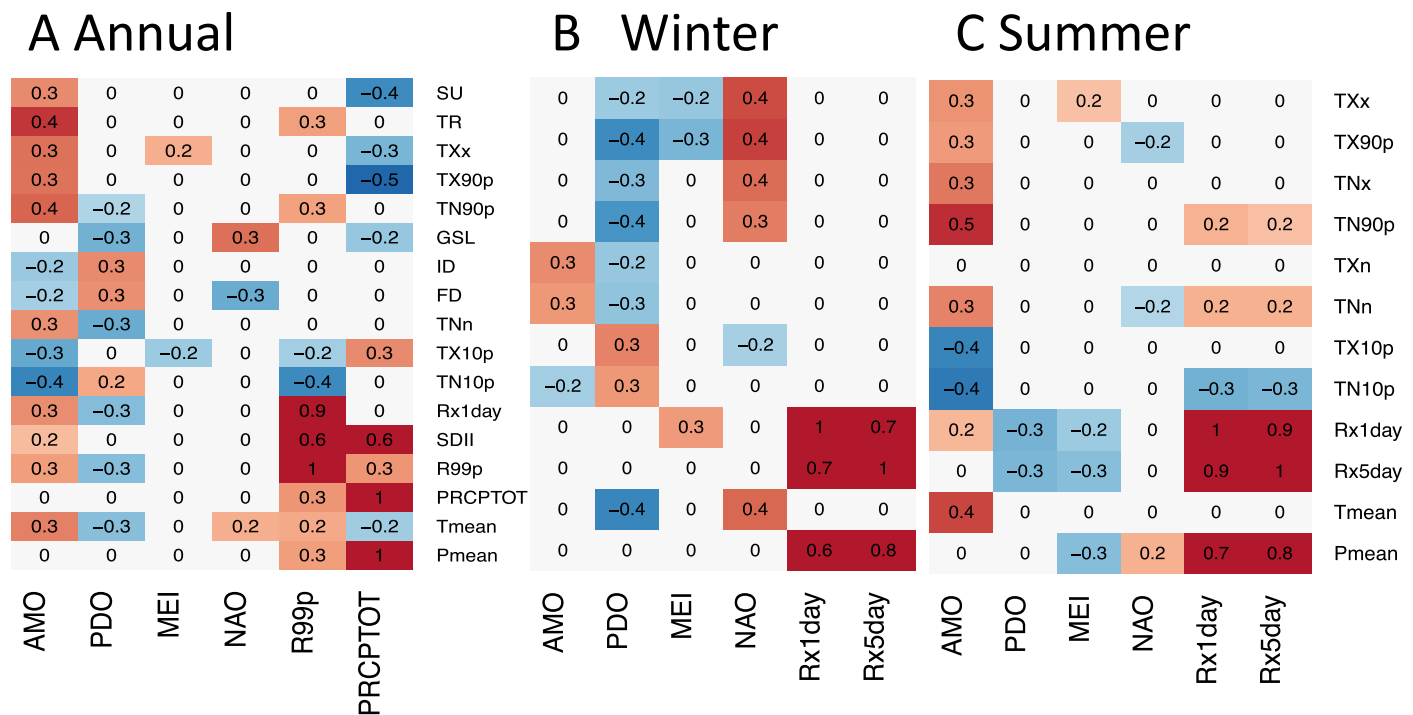
FIGURE 12. Cross-correlation between the indices and mean temperature (T_{mean}) and precipitation (P_{mean}) and the climate modes. Only statistically significant correlations are shown. (a) Annual indices, (b) Winter season climate indices. (c) Summer climate indices.

Janssen, et al. 2013; Kunkel, Stevens, Stevens, Sun, Wuebbles, et al. 2013; Jacobs et al. 2015) though the majority of these investigations have focused on watershed-size or regional analyses over large geographic scales. Large-scale assessments can result in more conservative changes due to the inclusion of heterogeneous weather station data such as those at higher elevations and/or further inland away from coastal storms impacts. Indeed, the HadEX2 product (Figure 1), which spans an area smaller than a typical state or regional analysis varies significantly from the patterns of climate extremes observed in the low-altitude near-shore regions of Chesapeake Bay. The Chesapeake Bay is centered at the union of the Northeast and Southeast U.S. regions, thus these averaged regional analyses do not accurately reflect the local climate of the near-shore region. The North and South Chesapeake regions described here illustrate consistent differences in the trends in climate extreme indices demonstrating that even at small spatial scales, climate patterns are heterogeneous.

Changes in cold events are highlighted in Northeast and Southeast U.S. climate assessments (Kunkel, Stevens, Stevens, Sun, Janssen, et al. 2013; Kunkel, Stevens, Stevens, Sun, Wuebbles, et al. 2013; Horton et al.), with both regions showing reductions in cold event frequency throughout the U.S. (Easterling 2002; Alexander et al. 2006; Brown et al. 2010;

Melillo et al. 2014; Romero-Lankao et al. 2014) with greater reductions occurring in the northern portion of their respective regions based on the dynamically downscaled North American Regional Climate Change Assessment Program (NARCCAP) model ensemble (http://www.narccap.ucar.edu/). Changes in FD frequency have been related to sea level pressure, in which a lower pressure increases cloudiness, as well as changes in regional circulation patterns (Meehl et al. 2004). FD decreases are larger in the Northeast (−26 and −32 days for the NARCCAP and CMIP3 model ensembles from 1985 to 2055) and smaller for the Southeast region (−17 and −18 days). Our observed changes are much smaller than the regional assessments (−6(−2) days in North(South) Chesapeake).

Changes in FD and minimum temperatures (TNn) are directly related to the length of the growing season in the Chesapeake Bay. GSL has been increasing globally with increases throughout the Northern Hemisphere (Peterson et al. 2001). In the Chesapeake Bay region, spring water temperatures have increased in the second half of the century expanding the aquatic GSL (Austin 2002; Preston 2004; Wood and Austin 2009). This increased duration of warm water could influence the phenological cues for organisms such as blue crab (*Callinectes sapidus*). Increased GSL in the Northern Hemisphere has been
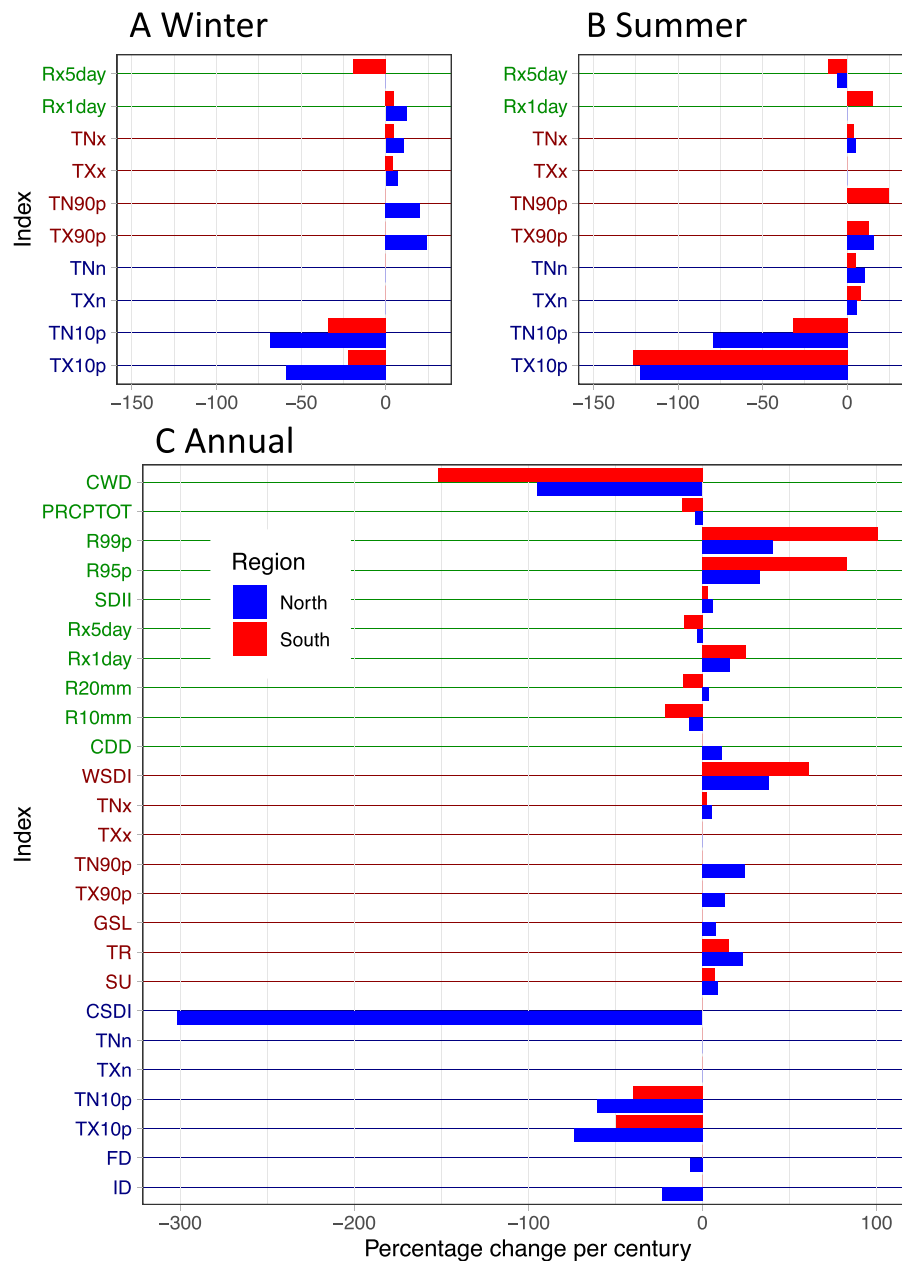
FIGURE 13. Summary percentage changes relative to the climate normal in the indices in Winter and Summer, and annually. Insignificant changes are not shown. Cool, warm, and precipitation-related indices are labeled in blue, red, and green, respectively.

correlated with reduced snow cover and an earlier disappearance of snow, leading to a hypothesis for a positive feedback mechanism between snow cover, surface albedo, and warming (Groisman et al. 1994). The Northeast Climate Assessment finds a significant increasing trend in a similar measure, the frost-free season, with a duration increase of roughly eight days over the period from 1900 to 2011 (Kunkel, Stevens, Stevens, Sun, Janssen, et al. 2013; Kunkel, Stevens, Stevens, Sun, Wuebbles, et al. 2013; Horton et al.). This is much smaller than our local GSL

increase of 23(7) days in the North(South) Chesapeake over a similar period. No significant trend in frost-free season was detected in the southeast climate assessment (Kunkel, Stevens, Stevens, Sun, Janssen, et al. 2013; Kunkel, Stevens, Stevens, Sun, Wuebbles, et al. 2013).

TR frequency, or the annual count of days when the daily minimum temperature >20°C (Table 1), has increased worldwide (Alexander et al. 2006; Sillmann and Roeckner 2008) with large increases in the U.S. Northeast region (Brown et al. 2010). These

nighttime summer temperature increases are not well understood, but are likely related to increases in cloudiness and atmospheric aerosols, and to changes in the atmospheric circulation variability (Karl et al. 1993; Easterling et al. 1997). Additional hypotheses include night-time warming caused by increased humidity and decreased soil moisture due to increasing evapotranspiration (Fischer and Schar 2010; Melillo et al. 2014). Brown et al. (2010) found an increase in TR of 1.1 days from 1893 to 2005 in the Northeast region, which is much smaller than the increases in the North(South) Chesapeake regions over a comparable time span, 9(8) days.

Globally, changes in precipitation intensity associated with climate change display a more spatially variable pattern with lower confidence in trends than temperature-based indices (Donat et al. 2013b). This is also evident at small scales, as demonstrated by the differences between the R99p (sum of the annual precipitation in events exceeding the daily 99th percentile) index for North and South Chesapeake regions. The historical increases are 4.1 mm per decade (41% per century) in the North and 9.8 mm per decade (101% per century) in the South Chesapeake regions (Table 4). This agrees only in sign with the large scale pattern in the National Climate Assessment which reports increases in R99p of 71% in the Northeast and 27% in the Southeast between 1958 and 2012 (Horton et al. 2014a; Melillo et al. 2014; Walsh et al. 2014). Note that the 1960s drought conditions may lead to estimation of higher trends in precipitation over the 54-year period than those we report for the full century, demonstrating that the length of the trend analysis can have a profound influence on the trend magnitude and assessment of significance. Observations, theory, and climate models attribute these changes in precipitation intensity to increased atmospheric temperatures leading to increases in the amount of moisture that can be held in the atmosphere and resulting intensification of the hydrological cycle (Kattenberg et al. 1996; Frei et al. 1998; Melillo et al. 2014).

Historical changes in seasonal precipitation over the region are not described in the climate assessments. Larger increases are observed in Rx5day precipitation in winter and summer in the South than the North (Table 4). Note that the HadEX2 past trends have a smaller magnitude than the North and South Chesapeake region trends which might indicate that the larger scale of the climate model grids plays a role in this discrepancy. The model projections are over a spatial scale more comparable to the HadEX2 gridded cell which could help to explain their lower sensitivity. Previous work has suggested that coastal regions have higher trends in extreme precipitation in the northeast U.S. (Brown et al.

2010), and this may also be a factor driving the higher trends in precipitation intensity described here.

Natural Climate Variability in the Historical Record

Natural climate variability in the form of large-scale climate modes and climate change associated with anthropogenic greenhouse gas emissions is co-occurring and may interact, changing the level of synoptic variability. Some modes of variability with the potential to influence climate near the Chesapeake Bay include NAO, AMO, PDO, and MEI (ENSO). The NAO describes the intensity of the atmospheric jet stream and westerlies which strongly influence the spatial distribution, intensity, and frequency of winter storms in the Atlantic sector (Visbeck et al. 2001 and references therin). During the positive phase of the NAO, conditions along the U.S. east coast are expected to be warmer and wetter than average. The AMO is a low frequency (65–80 year) cycle in Atlantic sea surface temperature that has been linked to hurricane frequency, changes in rainfall and streamflow in the U.S., and may also be related to fluctuations in the Atlantic Ocean meridional overturning circulation (Delworth and Mann 2000; Enfield et al. 2001). The PDO is a mode of variability centered in the Pacific with characteristic time scales of 15–20 years and 50–70 years (Mantua and Hare 2002). PDO and AMO have been linked to large-scale drought in the continental U.S. (McCabe et al. 2004). The MEI uses multiple atmospheric and oceanic measures to construct an index that describes the ENSO process in the tropical Pacific. ENSO and PDO have recently been shown to influence streamflow presumably through altering precipitation patterns over the Chesapeake Bay watershed (Schulte et al. 2016).

Many studies have highlighted the importance of caution in interpreting linear trends in climate time series (e.g., Woodward and Gray 1993; Liebmann et al. 2010) due to factors such as endpoint sensitivity, autocorrelation, and trend sensitivity to outliers; in addition to the recognition that climate change need not be linear. The nonparametric Mann–Kendall test and Sen's slope are less sensitive to outliers and skewed data distributions. However, the low-frequency oscillations present in the Mid-Atlantic region in the natural climate system can also bias estimation of the long-term trend if the length of the time series does not resolve the oscillation. For example, the AMO has nearly two full periods over the record of historical climate data in this study. Indices that are influenced by the AMO might mis-attribute the cyclic variability in the AMO to an increasing trend if the time series commences after 1940. This is exacerbated in this region because the PDO also has low-frequency variability, and time series

beginning later than 1950 could also mis-attribute PDO variability to climate change. Nonlinear climate responses that are potentially attributable to anthropogenic climate change may also cause trend estimation to be sensitive to the length of the climate record.

To quantify the sensitivity of our results to natural and nonlinear climate variability, the sensitivity of the annual indices linear trends to the length and starting point of the time series is calculated following Liebmann et al. (2010) (Figure 14). All three methods for computing trends show similar values that remained nearly constant through the first half of the century for temperature-based time series. Precipitation indices also show little change in trend through the first part of the century, though R20mm and PRCPTOT both show a consistent acceleration of the trend to increasing rainfall that intensifies midcentury. Nearly all the trends calculated from shortened time series experienced marked change commencing after 1940 with the exception of R95p. This is consistent with an increasing trend in global surface temperature as the starting point moves farther into the century (Liebmann et al. 2010). It is tempting to attribute the mid-century increase to intensification in the rate of global temperature rise. However, the period from 1930 to 1960 was anomalously warm and this apparently cyclical warm event, that appears to be associated with the AMO and PDO, is likely influencing trend estimates that commence mid-century. For precipitation-related indices, the 1960s was a period associated with a very strong drought in the U.S. Northeast during a period of an unusually persistent negative phase NAO (Seager et al. 2012). Thus, climate time series beginning after 1950 in this region will generally suggest larger changes in extreme events than we find using longer time series. Regardless of whether the trends in the climate extreme indices are due to anthropogenic climate change or natural variability, the environment of the Chesapeake Bay is currently experiencing accelerated change.

The correlations between large scale climate modes and climate extremes (Figure 12) are generally greater than the correlation between the climate modes and the average temperature and precipitation. In particular, the relationship between NAO and climate in this region may be expressed through changes in the frequency of storm events rather than through the intensification of storms. This is consistent with the positive NAO phase driving more mild winters along the east coast of the U.S., though the correlation with a mean temperature is less significant than for the FD and GSL indices. The NAO is not related to changes in precipitation or extremes in precipitation in this analysis in contrast to the broader regional patterns.

The positive ENSO phase appears to have a weak influence on annual scale temperature increases in this region, though this is again not reflected in mean temperature, but rather in the intensity of the highest annual temperatures. The negative PDO correlation with measures of annual precipitation intensity is consistent with the study of Schulte et al. (2016) and with other research noting its influence on drought. However, it was not correlated with annual average precipitation. The PDO projected more strongly on winter indices of warming and cooling, suggesting that its influence could lie in tempering the intensity of synoptic winter storm systems.

The relationship between the AMO and annual extremes is very strong and might be expected in a mode that manifests as elevated sea surface temperature. The annual relationship appears to be driven by summer rather than winter (Figure 12b,c). A positive correlation of AMO with elevated precipitation intensity could possibly reflect an intensification of the hydrological cycle associated with warmer ocean temperatures, but this is not found in average annual precipitation. A positive AMO phase and negative ENSO phase are associated with increased hurricane activity (Trenberth and Shea 2006), and so the correlation between AMO and summer and fall precipitation relationship could be associated with tropical storm activity.

Interestingly, the modes of variability are often more highly correlated with the extreme event indices than with the mean temperature and precipitation. In some cases, more than 40% of the variance is explained by large-scale climate modes. This suggests that the influence of these modes is likely changing the frequency of synoptic weather patterns that might lead to local extremes rather than a general warming or rainfall trend. In general, the climate modes tested here appear to have only moderate impacts on mean Chesapeake temperature and precipitation. However, the correlations in some cases are sufficient to suggest the potential of using these measures for forecasting.

The ecological and/or water quality implications of these temperature and rainfall extremes may also depend on their covariance. The negative correlations between summer precipitation intensity and cold event duration illustrated in Figure 12 and the positive correlations with warm event duration and temperature reflect that intense rainfall tended to occur when there were fewer nighttime low temperatures and more nighttime warm events. The co-occurrence of warm nighttime temperatures and high rainfall could lead to increases in Bay stratification co-occurring with freshwater input of nutrients from runoff. This could exacerbate hypoxia.
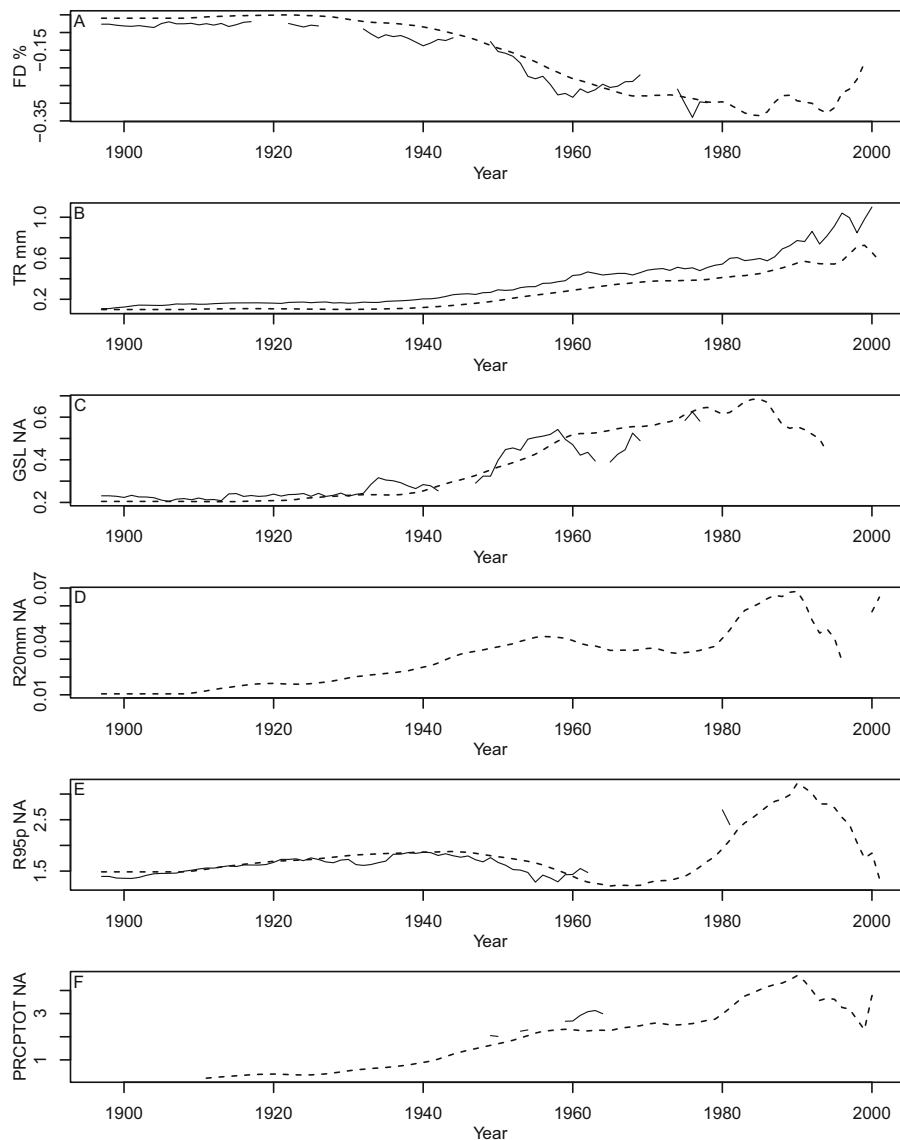
FIGURE 14. Change in linear trend per decade for each series as a function of time-series length. Trend per decade calculated from a given starting point to 2016 is plotted at the starting point. Solid lines show the raw time series, and dashed lines are calculated on the 21-year filtered time series, dotted lines are the Sen's trend. Only significant trends are shown. (a) FD (days/decade), (b) TR (days/decade), (c) GSL (days/decade), (d) R20mm (mm/decade), (e) R95p (mm/decade), (f) Total annual precipitation (mm/decade).

Local Relevance of Extreme Event Indices to Ecology and Water Quality

To provide some context for their use, here we demonstrate some consequences of changes in the climate extreme indices. In both regions and all seasons, nighttime daily maximum temperatures (TNx) increased. Failure to cool sufficiently in the evening can have significant human health impacts (Fischer and Schar 2010; Melillo et al. 2014; Lee et al. 2017) as well as feedback to increased air conditioning and energy usage that can significantly increase the local temperature in urban areas (Lundgren and Kjellstrom 2013). According to the National Weather Service, excessive heat events

are the number one cause of weather-related fatalities, and people are especially at risk when night temperatures remain above 70°F, the threshold for the TR index. Nighttime temperature increases are correlated with declines in crop yields including rice, corn, and soybean, possibly due to changes in temperature-related respiration rates (Peng et al. 2004).

A tight correlation between air and water temperatures in the Chesapeake Bay (Austin 2002; Ding and Elmore 2015) reflects close coupling of the atmospheric and estuarine boundary layers, and this is particularly the case in nearshore shallow waters with lower thermal mass. For example, the maximum daily temperature is strongly correlated with the

maximum daily water temperature at two NERR locations, Jug Bay in Maryland and Taskinas Creek in Virginia (2003–2015; Jug Bay adj. R^2 0.82, Taskinas Creek adj. R^2 0.76). Even at 15-min time scales, Jug Bay air and water temperatures are strongly correlated (adj. R^2 0.74). The thermal extreme indices presented here based on daily atmospheric temperature thus are relevant to the conditions experienced in the upper Chesapeake Bay water column in general, and to shallow regions in particular.

Warm summer nights are expected to worsen hypoxia in coastal environments by increasing respiration rates and decreasing oxygen saturation (Conley et al. 2009; Rabalais et al. 2009). The increase in warm nights suggests, as has been widely observed (Easterling et al. 1997), that the diurnal cycle is shifting, with local feedbacks limiting daytime highs, particularly in the south. Higher night-time temperatures could be indicative of increased humidity and cloud cover (Karl et al. 1993; Dai et al. 1999), but can also be due to intrinsic climate sensitivity associated with a thinner nighttime boundary layer (Davy et al. 2017).

Thresholds for reducing nutrient inputs stem from guidelines about reducing the duration and magnitude of low oxygen events. A primary driver for oxygen solubility is temperature, thus increased duration of high daily low temperature and daily high temperature (TN90p, TX90p) will act to reduce the oxygen concentration in the higher temperature water. However, the change in oxygen solubility at temperatures representative of summertime Chesapeake Bay conditions (e.g., 20–35°C) is small relative to the changes at lower wintertime temperatures. Additionally, as is well understood (Irby et al. 2018; Roman et al. 2019), chemical solubility is not the only factor driving oxygen dynamics in shallow coastal systems. Biological oxygen production is also temperature sensitive (Boyd et al. 2013) as is oxygen demand due to chemical oxidation processes and bacterial respiration. These are typically modeled as a function of temperature, with an ensemble of the Chesapeake Bay measurements suggesting stronger thermal sensitivity in bacterial production than primary production (Lomas et al. 2002). A recent synthesis of the response of the Chesapeake Bay hypoxia to climate change concludes that the duration of hypoxia will extend in response to warming, with hypoxic onset seven days earlier in spring (Irby et al. 2018), though as temperatures rise, biological oxygen demand may play a larger role.

Absolute concentration and duration of low oxygen (5 mg/L) concentration events did not correlate with any of the monthly indices of temperature or precipitation at Jug Bay. Indeed, the probability of low oxygen events was higher at intermediate water
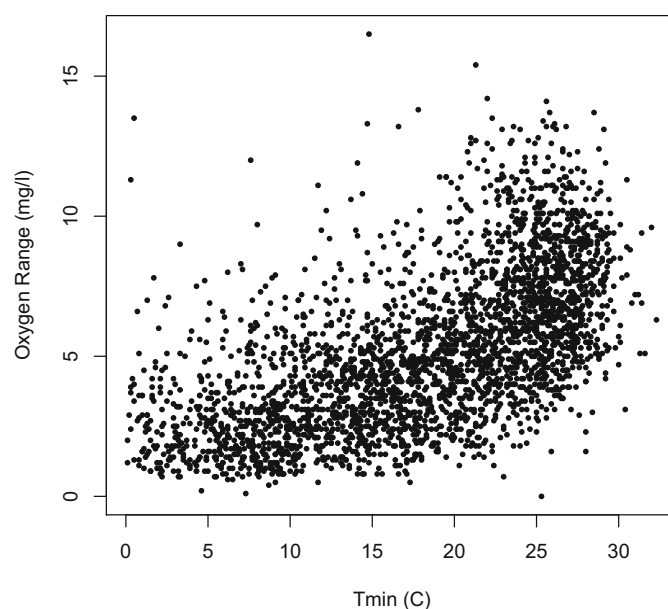

FIGURE 15. Relationship between diurnal oxygen range and the minimum daily temperature.

temperatures centered around 25°C in June-August. What does emerge as a significant relationship is a link between the diurnal range in oxygen concentration and nighttime minimum and daily maximum temperatures (Figure 15). More frequent warm events or higher daily temperatures (e.g., higher TX90p, TN90p, TXx, TXn) are associated with higher daytime oxygen values from high photosynthetic rates, as well as with stronger drops in nighttime oxygen concentration from the water column and sediment (benthic) respiration. Thus, in the Chesapeake Bay shallow regions, the diurnal range in oxygen expands with increasing thermal events. This expansion results in a higher probability that organisms will experience daily (chronic) periods of low oxygen stress as indices such as TX90p increase. The diurnal variation increase is associated with competing influences of decreasing oxygen solubility, increased primary production (increasing oxygen to potentially oversaturated levels), and increased respiration (drawing down oxygen concentration at night when primary production is halted).

CONCLUSIONS

The Chesapeake Bay estuary has already experienced significant increases in warm events and decreases in cold events, and these changes have been accelerating over the past 40–50 years (Figure 14). The annual precipitation quantity was

slightly decreased, with the southern portion of the Bay reporting greater change. However, measures of precipitation generally suggested an increase in annual precipitation intensity with seasonal measures significant only in the southern region. All these historical trends have a strong confidence level (4), suggesting that the Chesapeake Bay has undergone climate regime and environmental boundary shifts over the past century. Future projections using conservatively optimistic (RCP4.5) and "worst-case" (RCP8.5) emission scenarios suggest that these trends will continue over the next century.

The near-shore Chesapeake Bay region differs significantly from the Northeast and Southeast Regional Assessments (Kunkel, Stevens, Stevens, Sun, Janssen, et al. 2013) in many measures of climate variability over the past century. Projecting these changes into the future can be uncertain, as the model ensemble does not always replicate these patterns in the past. However, the model ensemble does consistently have the same trend direction between past and future.

This analysis focuses primarily on centennial trends to avoid aliasing climate modes (AMO, PDO, NAO, ENSO) that might project onto a secular trend. Analysis of the trend sensitivity to starting points demonstrates that most indices are changing more rapidly in the second half of the 20th Century, but historically natural variability in climate modes (some of which may be influenced by climate change) could be responsible for this intensification. Thus, locally focused climate syntheses should include more than a climate normal (30 years) in trend analyses when possible in order to identify the natural climate variability as well as the long-term trend.

Correlations between the extreme event indices and climate modes of variability over the past century indicate that the Chesapeake experiences cyclic climate changes in addition to secular trends. Significant relationships between modes of the AMO, PDO, MEI, and NAO and the extreme event indices are more common and often stronger than climate mode correlations with average temperature and precipitation patterns. This indicates potential predictability in climate extremes that may not be manifest in averages. It further highlights the need for research into how synoptic event distributions change as a result of these large-scale climate modes. Recent research has begun to suggest that Arctic sea ice loss and climate change are impacting the frequency and intensity of "blocking" events potentially leading to longer duration warm and cold events in mid-latitudes (Francis and Vavrus 2012; Chen et al. 2016; Coumou et al. 2018). While this analysis does not discriminate blocking events, a number of the climate extreme indices showed their largest extremes in the past decade, possibly consistent with such an increase.

This analysis highlights the importance of using local climate records to assess historical trends in both mean and extreme events. We provide the historical and future projections (also presented in Supporting Information) as a resource for further studies on climate impacts in the Chesapeake region. These observed trends also provide a means of evaluating the local skill of climate models and aid in assessing confidence in future projections.

Graphs and text files illustrating each index for historical data and future model projections are found in Supporting Information.

SUPPORTING INFORMATION

Additional supporting information may be found online under the Supporting Information tab for this article: Figures illustrating all the extreme indices analyzed.

AUTHORS' CONTRIBUTIONS

Kari A. St.Laurent: Data curation; formal analysis; methodology; software; validation; visualization; writing-original draft; writing-review & editing. **Victoria J. Coles:** Conceptualization; data curation; formal

analysis; funding acquisition; investigation; methodology; software; supervision; validation; visualization; writing-original draft; writing-review & editing. **Raleigh R. Hood:** Conceptualization; funding acquisition; methodology; project administration; supervision; writing-review & editing.

LITERATURE CITED

Alexander, L.V., X. Zhang, T.C. Peterson, J. Caesar, B. Gleason, A.M.G. Klein Tank, M. Haylock et al. 2006. "Global Observed Changes in Daily Climate Extremes of Temperature and Precipitation." *Journal of Geophysical Research* 111: D05109.

Austin, H.M. 2002. "Decadal Oscillations and Regime Shifts, a Characterization of the Chesapeake Bay Marine Climate." *American Fisheries Society Symposium* 32: 155–70.

Boyd, P.W., T.A. Rynearson, E.A. Armstrong, F. Fu, K. Hayashi, Z. Hu, D.A. Hutchins et al. 2013. "Marine Phytoplankton Temperature versus Growth Responses from Polar to Tropical Waters — Outcome of a Scientific Community-Wide Study." *PLoS One* 8: e63091. https://doi.org/10.1371/journal.pone.0063091.

Bronaugh, D. 2018. "climdex.pcic: PCIC Implementation of Climdex Routines." R Package, Version 1.1-9.1 https://mran.microsoft.com/snapshot/2019-12-26/web/packages/climdex.pcic/index.html.

Brown, P.J., R.S. Bradley, and F.T. Keimig. 2010. "Changes in Extreme Climate Indices for the Northeastern United States, 1870–2005." *Journal of Climate* 23: 6555–72.

Carter, L.M., J.W. Jones, L. Berry, V. Burkett, J.F. Murley, J. Obeysekera, P.J. Schramm, and D. Wear. 2014. "Chapter 17: Southeast and the Caribbean: Climate Change Impacts in the United States: The Third National Climate Assessment." U.S. Global Change Research Program, 396–417.

Chen, H.W., F. Zhang, and R.B. Alley. 2016. "The Robustness of Midlatitude Weather Pattern Changes Due to Arctic Sea Ice Loss." *Journal of Climate* 29: 7831–49.

Claggett, P.R., F.M. Irani, and R.L. Thompson. 2013. "Estimating the Extent of Impervious Surfaces and Turf Grass across Large Regions." *Journal of the American Water Resources Association* 49 (5): 1057–77.

Conley, D.J., J. Carstensen, R. Vaquer-Sunyer, and C.M. Duarte. 2009. "Ecosystem Thresholds with Hypoxia." *Hydrobiologia* 629: 21–29.

Coumou, D., G. Di Capua, S. Vavrus, L. Wang, and S. Wang. 2018. "The Influence of Arctic Amplification on Mid-Latitude Summer Circulation." *Nature Communications* 9. https://doi.org/10.1038/s41467-018-05256-8.

Dai, A., K.E. Trenberth, and T.R. Karl. 1999. "Effects of Clouds, Soil Moisture, Precipitation, and Water Vapr on Diurnal Temperature Range." *Journal of Climate* 12: 2451–73.

Davy, R., I. Esau, A. Chernokulsky, S. Outten, and S. Zilitinkevich 2017. "Diurnal Asymmetry to the Observed Global Warming." *International Journal of Climatology* 37: 79–93.

Delworth, T., and M.E. Mann. 2000. "Observed and Simulated Multi Decadal Variability in the Northern Hemisphere." *Climate Dynamics* 16: 661–76.

Ding, H., and A.J. Elmore. 2015. "Spatio-Temporal Patterns in Water Surface Temperature from Landsat Time Series Data in the Chesapeake Bay, U.S.A." *Remote Sensing of Environment* 168: 335–48.

Donat, M.G., L.V. Alexander, H. Yang, I. Durre, R.S. Vose, and J. Caesar. 2013a. "Global Land-Based Datasets for Monitoring Climatic Extremes." *Bulletin of the American Meteorological Society* 94: 997–1006.

Donat, M.g., L.v. Alexander, H. Yang, I. Durre, R. Vose, R.j.h. Dunn, K.m. Willett et al. 2013b. "Updated Analyses of Temperature and Precipitation Extreme Indices since the Beginning of the Twentieth Century: The HadEX2 Dataset." *Journal of Geophysical Research: Atmospheres* 118: 2098–118.

Easterling, D.R. 2002. "Recent Changes in Frost Days and the Frost-Free Season in the United States." *Bulletin of the American Meteorological Society* 83: 1327–32.

Easterling, D.R., B. Horton, P.D. Jones, T.C. Peterson, T.R. Karl, D.E. Parker, M.J. Salinger et al. 1997. "Maximum and Minimum Temperature Trends for the Globe." *Science* 277: 364–67.

Easterling, D.R., K.E. Kunkel, J.R. Arnold, T. Knutson, A.N. LeGrande, L.R. Leung, R.S. Vose, D.E. Waliser, and M.F. Wehner. 2017. "Precipitation Changes in the United States." In *Fourth National Climate Assessment* (Volume I), edited by D.J. Wuebbles, D.W. Fahey, K.A. Hibbard, D.J. Dokken, B.C. Stewart, and T.K. Maycock, 207–30. Washington, D.C.: U.S. Global Change Research Program.

Enfield, D.B., A.M. Mestas-Nunez, and P.J. Trimble. 2001. "The Atlantic Multidecadal Oscillation and Its Relation to Rainfall and River Flows in the Continental U.S." *Geophysical Research Letters* 28: 2077–80.

Fischer, E.M., and C. Schar. 2010. "Consistent Geographical Patterns of Changes in High-Impact European Heatwaves." *Nature Geoscience* 3: 398–403.

Francis, J.A., and S.J. Vavrus. 2012. "Evidence Linking Arctic Amplification to Extreme Weather in Mid-Latitudes." *Geophysical Research Letters* 39: 1–6.

Frei, C., C. Schär, D. Lüthi, and H.C. Davies. 1998. "Heavy Precipitation Processes in a Warmer Climate." *Geophysical Research Letters* 25: 1431.

Groisman, P.Y., T.R. Karl, and R.W. Knight. 1994. "Observed Impact of Snow Cover on the Heat Balance and the Rise of Continental Spring Temperatures." *Science* 263: 198–200.

Horton, R., G. Yohe, W. Easterling, R. Kates, M. Ruth, E. Sussman, A. Whelchel, D. Wolfe & Lipschultz, F. 2014a. "Ch. 16: Northeast." In *Climate Change Impacts in the United States: The Third National Climate Assessment*, edited by J.M. Melillo, T.C. Richmond, and G.W. Yohe, U.S. Global Change Research Program, 371–95.

Hurrell, J.W., Y. Kushnir, G. Ottersen, and M. Visbeck. 2003. "An Overview of the North Atlantic Oscillation." In *The North Atlantic Oscillation: Climatic Significance and Environmental Impact*, edited by J.W. Hurrell, Y. Kushnir, G.G. Ottersen, and M. Visbeck, 1–35. Washington, D.C.: American Geophysical Union.

IPCC. 2014. "Climate Change 2014: Synthesis Report." In *Contribution of Working Groups I, II and III to the Fifth Assessment Report of the Intergovernmental Panel on Climate Change*, edited by Core Writing Team, R.K. Pachauri, and L.A. Meyer, 1–168. Geneve, Switzerland: IPCC.

Irby, I.D., M.A.M. Friedrichs, F. Da, and K.E. Hinson. 2018. "The Competing Impacts of Climate Change and Nutrient Reductions on Dissolved Oxygen in Chesapeake Bay." *Biogeosciences* 15: 2649–68.

Jacobs, J., S.K. Moore, K.E. Kunkel, and L. Sun. 2015. "A Framework for Examining Climate-Driven Changes to the Seasonality and Geographical Range of Coastal Pathogens and Harmful Algae." *Climate Risk Management* 8: 16–27.

Karl, T.R., P.D. Jones, R.W. Knight, G. Kukla, N. Plummer, V. Razuvayev, K.P. Gallo, J. Lindseay, R.J. Charlson, and T.C. Peterson. 1993. "Asymmetric Trends of Daily Maximum and Minimum Temperature." *Bulletin of the American Meteorological Society* 74: 1007–23.

Karl, T.R., J.M. Melillo, and T.C. Peterson. 2009. *Global Climate Change Impacts in the United States*. New York, NY: Cambridge University Press.

Karl, T.R., N. Nicholls, and A. Ghazi. 1999. "CLIVAR/GCOS/WMO Workshop on Indices and Indicators for Climate Extremes —

Workshop Summary." *Weather and Climate Extremes*: 42: 3–7. https://doi.org/10.1007/978-94-015-9265-9_2.

Kattenberg, A., F. Giorgi, H. Grassl, G.A. Meehl, J.F. Michelle, R. Stouffer, T. Tokioka, A.J. Weaver, and T.M. Wigley. 1996. "Climate Models-Projections and Future Climate. The Science of Climate Change." Contribution of Working Group I to the Second Assessment Report of the Intergovernmental Panel on Climate Change, 285–357.

Kemp, W.M., W.R. Boynton, J.E. Adolf, D.F. Boesch, W.C. Boicourt, G. Brush, J.C. Cornwell *et al*. 2005. "Eutrophication of Chesapeake Bay: Historical Trends and Ecological Interactions. Marine Ecology Progress Series." *Marine Ecology Progress Series* 303: 1–29.

Kunkel, K.E., L. Stevens, S. Stevens, L. Sun, E. Janssen, D. Wuebbles, S. Hilberg *et al*. 2013. "Regional Climate Trends and Scenarios for the U.S. National Climate Assessment." NOAA Technical Report NESDIS 142-2.

Kunkel, K.E., L.E. Stevens, S.E. Stevens, L. Sun, D. Wuebbles, E. Janssen, J. Rennells, A. DeGaetano, and J.G. Dobson. 2013. "Regional Climate Trends and Scenarios for the U.S. National Climate Assessment Part 1. Climate of the Northeast U.S." NOAA Technical Report NESDIS 142-1.

Lee, W.H., Y.H. Lim, T.N. Dang, X. Seposo, Y. Honda, Y.L.L. Guo, H.M. Jang, and H. Kim. 2017. "An Investigation on Attributes of Ambient Temperature and Diurnal Temperature Range on Mortality in Five East-Asian Countries." *Scientific Reports* 7: 1–9.

Liebmann, B., R.M. Dole, C. Jones, I. Bladé, and D. Allured. 2010. "Influence of Choice of Time Period on Global Surface Temperature Trend Estimates." *Bulletin of the American Meteorological Society* 91: 1485–91.

Lomas, M.W., P.M. Glibert, F.K. Shiah, and E.M. Smith. 2002. "Microbial Processes and Temperature in Chesapeake Bay: Current Relationships and Potential Impacts of Regional Warming." *Global Change Biology* 8: 51–70.

Lundgren, K., and T. Kjellstrom. 2013. "Sustainability Challenges from Climate Change and Air Conditioning Use in Urban Areas." *Sustainability* 5: 3116–28.

Lusk, S.C., B.E. Watkins, A. Rhea, C.B. Dillman, E.J. Hilton, S.C. Lusk, and B.E. Watkins. 2014. "Occurrence of Juvenile Paralichthys Lethostigma (Southern Flounder) in Tributaries of Chesapeake Bay." *Southeastern Naturalist* 13: 515–22.

Mantua, N.J., S.R. Hare, and Y. Zhang. 1997. "A Pacific Interdecadal Climate Oscillation with Impacts on Salmon Production." *Bulletin of the American Meteorological Society* 78 (6): 1069–79.

Mantua, N.J., and S.R. Hare. 2002. "The Pacific Decadal Oscillation." *Journal of Oceanography* 58: 35–44.

Maraun, D., T.G. Shepherd, M. Widmann, G. Zappa, D. Walton, J.M. Gutiérrez, S. Hagemann *et al*. 2017. "Towards Process-Informed Bias Correction of Climate Change Simulations." *Nature Climate Change* 7: 764–73.

McCabe, G.J., M.A. Palecki, and J.l. Betancourt. 2004. "Pacific and Atlantic Ocean Influences on Multidecadal Drought Frequency in the United States." *Proceedings of the National Academy of Sciences of the United States of America* 101: 4136–41.

McLeod, A.I. 2011. "Kendall Rank Correlation and Mann-Kendall Trend Test"." R Package Version 2.2. https://cran.r-project.org/web/packages/Kendall/Kendall.pdf.

Meehl, G.A., C. Tebaldi, and D. Nychka. 2004. "Changes in Frost Days in Simulations of Twentyfirst Century Climate." *Climate Dynamics* 23: 495–511.

Melillo, J.M., T.C. Richmond, and G.W. Yohe, (Eds). 2014. "Climate Change Impacts in the United States: The Third National Climate Assessment." U.S. Global Change Research Program, 841 pp.

Moore, K.A., and J.C. Jarvis. 2008. "Eelgrass Diebacks in the Lower Chesapeake Bay: Implications for Long-Term Persistence." *Journal of Coastal Research* 55: 135–47.

Moss, R.H., J.A. Edmonds, K.A. Hibbard, M.R. Manning, S.K. Rose, D.P. Van Vuuren, T.R. Carter *et al*. 2010. "The Next Generation of Scenarios for Climate Change Research and Assessment." *Nature* 463: 747–56.

Najjar, R.G., C.R. Pyke, M. Adams, D.L. Breitburg, C. Hershner, M. Kemp, R. Howarth *et al*. 2010. "Potential Climate-Change Impacts on the Chesapeake Bay." *Estuarine, Coastal and Shelf Science* 86: 1–20.

Peng, S., J. Huang, J.E. Sheehy, R.C. Laza, R.M. Visperas, X. Zhong, G.S. Centeno, G.S. Khush, and K.G. Cassman. 2004. "Rice Yields Decline with Higher Night Temperature from Global Warming." *Proceedings of the National Academy of Sciences of the United States of America* 101: 9971–75.

Peterson, T.C., C. Folland, G. Gruza, W. Hogg, N. Plummer, A. Mokssit, and N. Plummer. 2001. "Report on the Activities of the Working Group on Climate Change Detection and Related Rapporteurs 1998–2001." WMO, Rep. WCDMP-47,WMO-TD 1071, International CLIVAR Project Office, Geneve, Switzerland.

Pohlert, T. 2018. "Trend: Non-Parametric Trend Tests and Change Point Detection." The Comprehensive R Archive Network (CRAN), Version 1.1.1.

Preston, B.L. 2004. "Observed Winter Warming of the Chesapeake Bay Estuary (1949–2002): Implications for Ecosystem Management." *Environ. Assessment* 34: 125–39.

Pyke, C.R., R.G. Najjar, M.B. Adams, D.L. Breitburg, M. Kemp, C. Hershner, R. Howarth, M. Mulholland, M. Paolisso, and D. Secor. 2008. "Climate Change and the Chesapeake Bay: State-of-the-Science Review and Recommendations." A Report from the Chesapeake Bay Program Science and Technical Advisory Committee (STAC), Annapolis, MD, 59: 29–40.

Rabalais, N.N., R.E. Turner, R.J. Díaz, and D. Justić. 2009. "Global Change and Eutrophication of Coastal Waters." *ICES Journal of Marine Science* 66: 1528–37.

Roman, M.R., S.B. Brandt, E.D. Houde, and J.J. Pierson. 2019. "Interactive Effects of Hypoxia and Temperature on Coastal Pelagic Zooplankton and Fish." *Frontiers in Marine Science* 6: 1–18.

Romero-Lankao, P., J.B. Smith, D.J. Davidson, N.S. Diffenbaugh, P.L. Kinney, P. Kirshen, P. Kovacs, and L. Villers-Ruiz. 2014. "North America. Climate Change 2014: Impacts, Adaptation, and Vulnerability. Part B: Regional Aspects." Contribution of Working Group II to the Fifth Assessment Report of the Intergovernmental Panel of Climate Change. http://thuvienso.vanlanguni.edu.vn/handle/Vanlang_TV/10063.

Scholz, F., and A. Zhu. 2019. "K-Sample Rank Tests and their Combinations." The Comprehensive R Archive Network (CRAN), Version 1.2-9 https://cran.r-project.org/web/packages/kSamples/kSamples.pdf.

Schulte, J.A., R.G. Najjar, and M. Li. 2016. "Regional Studies the Influence of Climate Modes on Streamflow in the Mid-Atlantic Region of the United States." *Journal of Hydrology* 5: 80–99.

Seager, R., N. Pederson, Y. Kushnir, J. Nakamura, and S. Jurburg. 2012. "The 1960s Drought and the Subsequent Shift to a Wetter Climate in the Catskill Mountains Region of the New York City Watershed." *Journal of Climate* 25: 6721–42.

Sillmann, J., V.V. Kharin, X. Zhang, F.W. Zwiers, and D. Bronaugh. 2013. "Climate Extremes Indices in the CMIP5 Multimodel Ensemble: Part 1. Model Evaluation in the Present Climate." *Journal of Geophysical Research: Atmospheres* 118: 1716–33.

Sillmann, J., and E. Roeckner. 2008. "Indices for Extreme Events in Projections of Anthropogenic Climate Change." *Climatic Change* 86: 83–104.

Tebaldi, C., J.M. Arblaster, and R. Knutti. 2011. "Mapping Model Agreement on Future Climate Projections." *Geophysical Research Letters* 38: 1–5.

Trenberth, K.E., and D.J. Shea. 2006. "Atlantic Hurricanes and Natural Variability in 2005." *Geophysical Research Letters* 33: 1–4.

Visbeck, M.H., J.W. Hurrell, L. Polvani, and H.M. Cullen. 2001. "North Atlantic Oscillation: Past, Present, and Future." *Proceedings of the National Academy of Sciences of the United States of America* 98: 12876–77.

Vose, R.S., D.R. Easterling, K.E. Kunkel, A.N. LeGrande, and M.F. Wehner. 2017. "Temperature Changes in the United States." In *Forth National Climate Assessment* (Volume I), edited by D.J. Wuebbles, D.W. Fahey, K.A. Hibbard, D.J. Dokken, B.C. Stewart, and T.K. Maycock, 185–206. Washington, D.C.: U.S. Global Change Research Program.

Walsh, J., D. Wuebbles, and K. Hayhoe. 2014. "Chapter 2: Our Changing Climate. Climate Change Impacts in the United States: The Third National Climate Assessment." 19–67. https://doi.org/10.7930/J0KW5CXT

Wang, J., A. Dai, and C. Mears. 2016. "Global Water Vapor Trend from 1988 to 2011 and Its Diurnal Asymmetry Based on GPS, Radiosonde, and Microwave Satellite Measurements." *Journal of Climate* 29: 5205–22.

Wei, T., and V. Simko. 2021. "R package 'corrplot': Visualization of a Correlation Matrix", Version 0.90. https://github.com/taiyun/corrplot.

Wolter, K., and M.S. Timlin. 1998. "Measuring the Strength of ENSO Events: How Does the 1997/8 Rank?" *Weather* 53: 315–24.

Wood, R.J., and H.M. Austin. 2009. "Synchronous Multidecadal Fish Recruitment Patterns in Chesapeake Bay, USA." *Canadian Journal of Fisheries and Aquatic Sciences* 66: 496–508.

Woodward, W.A., and H.L. Gray. 1993. "Global Warming and the Problem of Testing for Trends in Time Series Data." *Journal of Climate* 6: 953–62.

Zeileis, A., and G. Grothendieck. 2005. "zoo: S3 Infrastructure for Regular and Irregular Time Series." *Journal of Statistical Software* 14: 1–27. https://doi.org/10.18637/jss.v014.i06.

Zhang, X., L.V. Alexander, G.C. Hegerl, P. Jones, A.K. Tank, T.C. Peterson, B. Trewin, and F.W. Zwiers. 2011. "Indices for Monitoring Changes in Extremes Based on Daily Temperature and Precipitation Data." *Wiley Interdisciplinary Reviews: Climate Change* 2: 851–70.

R package 'corrplot': Visualization of a Correlation Matrix